Residual Stresses and Properties of Layered and Graded Coatings

by

Olivera E. Kesler

Submitted to the Department of Materials Science and Engineering
in partial fulfillment of the requirements for the degree of

Doctor of Science in Materials Science

at the

MASSACHUSETTS INSTITUTE OF TECHNOLOGY

September 1999

Author .....
Department of Materials Science and Engineering
Aug 6, 1999

Certified by .....
Subra Suresh
R. P. Simmons Professor of Materials Science and Engineering
Thesis Supervisor

Accepted by .....
Linn W. Hobbs
John F. Elliott Professor of Materials and Chairperson, Department
Committee on Graduate Students

Residual Stresses and Properties of Layered and Graded Coatings

by

Olivera E. Kesler

Submitted to the Department of Materials Science and Engineering
on Aug 6, 1999, in partial fulfillment of the
requirements for the degree of
Doctor of Science in Materials Science

Abstract

The thermo-mechanical properties and residual stresses of various layered and graded coating materials were studied to gain a better understanding of thick coatings used in a variety of applications, including thermal barrier coatings, wear resistant coatings, and corrosion barriers. A new technique based on curvature measurements and successive build-up of layers of the coating was developed in order to allow the convenient and accurate determination of stresses and properties of thick and/or graded coatings, in order to complement previous work on thin films and thick homogeneous coatings. The new technique allows the determination of processing-induced residual stresses, Young's modulus, and coefficient of thermal expansion through the thickness of the coating, and also as a function of temperature at any given thickness position. The new technique was used, along with x-ray diffraction, neutron diffraction, and instrumented sharp indentation, to evaluate the properties of a variety of coating material systems. The material systems studied include Ni-Al_2O_3, NiCrAlY-ZrO_2, and homogeneous Mo coatings produced by plasma spray deposition on steel substrates. The through-thickness residual stresses in the coatings were determined, along with the variation of the coefficient of thermal expansion as a function of composition, and the Young's modulus. The influence of the two main factors contributing to the overall residual stresses in the coatings were also separated and calculated quantitatively: the thermal mismatch stress between the coating and substrate upon cooling from the deposition temperature to room temperature, and the quenching stress due to initial solidification of the coating on the substrates. A better understanding of the properties of thick layered and graded coatings was achieved, and guidelines for the experimental determination and optimization of coatings stresses and properties are presented.

Thesis Supervisor: Subra Suresh

Title: R. P. Simmons Professor of Materials Science and Engineering

Contents

List of Figures

List of Tables

Acknowledgements

I would like to take this opportunity to gratefully acknowledge the many people who have offered me their help and support during the period of this thesis work.

First of all, I would like to thank my thesis supervisor, Prof. Subra Suresh, for his encouragement, support, generosity, inspiration, understanding, and expert guidance throughout this work. It has truly been a privilege and a pleasure to work with him, and I am grateful for the opportunity to have worked in LEXCOM (Laboratory for Experimental and Computational Micromechanics) with him.

I would also like to thank Prof. Sanjay Sampath of the State University of New York at Stony Brook (SUNYSB) for his professional collaboration, for his frequent valuable input and suggestions, for his expertise and the use of his thermal spray facilities, and for all of his professional advice and encouragement.

Thank you to Prof. S. Mark Spearing and Prof. Ronald Latanision for their valuable and helpful suggestions for this work and for serving on my thesis committee. Thank you to Dr. Marc Finot for his friendship, encouragement, support, inspiration, collaboration, and many helpful discussions. Thank you to Dr. Jiri Matejicek of SUNYSB for his collaboration with the diffraction experiments. Thank you to Dr. Antonios Giannakopoulos for his encouragement, inspiration, and helpful discussions. Thank you to Ms. Krystyn Van Vliet for her friendship and support, and for her work on the calibration of the indentation equipment. Thank you to Mr. William Smith and Mr. Glenn Bancke of SUNYSB for help with the plasma spray deposition of the coatings. Thank you to Mr. Måns Mångård of Linköpings Universitet, Sweden, for his work on the CT scans of the specimens and his generous hospitality. Thank you to Mr. George Labonte, research specialist at LEXCOM, for his friendly encouragement and experimental assistance. Thank you to Mr. Kenneth Greene and Ms. Gloria Landahl for their friendly administrative help.

Thank you to all of my many colleagues, past and present, in LEXCOM for their support, help, and friendship, and for creating the professional atmosphere that has

made LEXCOM such a wonderful place to work.

Thank you to my colleagues at the Idaho National Engineering and Environmental Laboratory (INEEL), SUNYSB, and in the thermal spray and residual stress communities worldwide, for their valuable discussions, inspiration, and warm hospitality.

Thank you to the friends and colleagues at MIT who have made my time in graduate school so much more enjoyable.

Thank you to my colleagues and professors from the University of Pennsylvania's Department of Materials Science and Engineering for their friendship, inspiration, encouragement, support, knowledge, and for instilling in me a passion for the field. It is they who inspired me to continue my education in this field, and I am grateful for the lasting impact that they have had on my life and my career.

Thanks to the National Defense Science and Engineering Graduate Fellowship, INEEL, and National Science Foundation for making this work possible with their financial support. The work was supported by the INEEL Grant Agreement No. C95-175002-LKK-267-95, and the MRSEC program of the NSF, under award DMR-9632570, both of which were jointly funded at MIT and SUNYSB.

Finally, thank you to all of my wonderful friends and family members for their love and support and encouragement through the years. Their love has made me truly wealthy in the most important sense of the word, and for that, I will be forever grateful.

" Where the mind is without fear and the head is held high; Where knowledge is free; Where the world has not been broken up into fragments by narrow domestic walls; Where words come out from the depths of truth; Where tireless striving stretches its arms towards perfection; Where the clear stream of reason has not lost its way into the dreary desert sand of dead habit; Where the mind is led forward by thee into ever-widening thought and action - Into that heaven of freedom, my father, let my country awake." -Rabindranath Tagore

"I will act as if what I do makes a difference." -William James

Chapter 1

Introduction

1.1 Background

Thick coatings, with layer thicknesses of tens of micrometers to several millimeters, and thin-film coatings with layer thicknesses of tens of nanometers to several micrometers, are commonly used in a broad range of engineering components and electronic devices. Structural coatings are used, for example, as protective layers to guard against thermal, environmental, corrosive, tribological or mechanical degradation of metallic structures, and as layered electrodes and electrolytes in fuel cells [1-4]. The use of coating materials in these applications can have significant environmental benefits because their use can result in longer component lifetimes of the materials, and more efficient operating conditions, thus saving energy and reducing material waste. Thin films are used in such optical and communications applications as anti-reflective coatings on lenses, conductive metallic coatings on Si substrates in electronic devices, and thin magnetic coatings on metallic or polymeric substrates in information storage devices. [1]. The wide range of applications of different types of material coatings creates the necessity to understand the mechanical, thermal, and microstructural behavior of the coating materials, in order to better design the coatings to optimize their properties and to reliably predict their behavior.

Advances in processing methods such as chemical vapor deposition, physical vapor deposition, thermal spray, powder metallurgy, computer-aided three-dimensional printing, self-propagating high-temperature combustion synthesis, electron-beam deposition and molecular beam epitaxy have given rise to newer opportunities for the synthesis of thick- and thin-film layered coatings [5]. In addition to surface coatings with homogeneous compositions which produce sharp interfaces among dissimilar solids, there is a growing interest in functionally graded materials (FGM's) wherein gradual changes in composition among dissimilar solids are produced across interfaces. The processing methods above provide possibilities for controlling the spatial variation of composition and material properties across the coatings. The geometries of the graded interlayers in functionally graded material coatings are chosen to optimize the material behavior. Compared to sharp interfaces between dissimilar materials, for example, graded interfaces can mitigate internal stresses, enhance interfacial bonding, optimize the distribution of stresses and crack initiation sites, suppress the severity of stress concentrations at edges where interfaces intersect free surfaces, delay the onset of damage and yielding, allow the building of "thick" coatings (of thickness greater than or equal to approximately 2 mm) that would not be possible without grading, control the density and kinetics of misfit/threading dislocations emanating from interfaces, supression of surface damage and cracking during indentation, tribological contact, impact, and penetration, or to control the kinetics of diffusion and electrical conductivity across the materials [6-11].

All processing methods used to deposit surface coatings on substrates invariably generate intrinsic or residual stresses that are present in the coatings prior to any in-service loadings. These internal residual stresses, which strongly depend on the specific deposition conditions and processing methods employed, arise in plasma spray processing from such factors as: the rapid quenching of a molten droplet onto a substrate, non-uniform sintering of the material across the thickness of the coating, non-equilibrium cooling of the different phases, and epitaxial misfit strains. These factors

that create stresses during the creation or deposition of the coatings are referred to collectively in this work as the quenching stress. In addition, temperature excursions cause thermal stresses to develop due to expansion or contraction mismatch between the constituent phases within a layer or between layers, and between the deposited coating layers and the substrate. These thermal mismatch stresses combine with the quenching stresses to create a residual stress state in the coatings after the deposition process is completed, and before the coatings enter service. A knowledge of these intrinsic processing stresses is crucial in designing coating materials that can withstand a prescribed in-service loading stress without failure. In addition, knowledge of the connection between the processing conditions and the resulting values of residual stresses can be used to alter the processing conditions in order to minimize or optimize the initial stress state in the materials before they enter service. For example, spallation of a coating prior to a part entering service can be minimized by adjusting the processing conditions to optimize the residual stress state in the coating, for example, by introducing a residual compressive stress when possible.

The importance of understanding and optimizing the initial residual stress state in coatings has resulted in widespread efforts to evaluate these stresses [12,13]. The techniques that have been developed have different conditions for which they are most useful, accurate, and valid, as well as different levels of cost and experimental accessibility, convenience, and complexity. Thus, a range of techniques is useful in order to fully analyze a wide range of materials with different geometries and processing histories.

The goal of this work was to contribute to the understanding of thick layered and graded coatings by meeting the following objectives:

1. to determine the residual stresses and thermo-mechanical properties in a variety of layered materials, and for the first time in functionally graded materials.

2. to determine quantitatively the contributions of different components to the total residual stress.

3. to develop new methodologies for evaluation of stresses and properties in thick and/or graded coating materials that are relatively simple to implement.

4. to verify experimentally the new methodologies by using them to evaluate the residual stresses and properties of coating materials.

5. to assess the merits of the new methods developed in this work by comparing with other established methods.

6. to use the results obtained through residual stress and property determinations in order to better understand the behavior of coating materials and to determine practical methods of optimizing their properties.

1.2 Organization of the thesis

- Chapter 2 introduces a new methodology for determining residual stresses in layered or graded materials by use of successive build-up of material layers coupled with curvature measurements, and some preliminary experimental results using this method to determine the stresses and properties of a model coating system (Ni-Al_2O_3.)

- Chapter 3 uses the newly developed technique in order to determine stresses in a range of coating-susbstrate systems: Ni-Al_2O_3, NiCrAlY-ZrO_2, and Mo on steel substrates. These same material systems are also examined using two other commonly used methods for determining residual stresses: x-ray diffraction and neutron diffraction. Experimental results obtained using all three techniques for a variety of coating-substrate systems are presented and compared. The implications of the results are discussed in terms of the conditions under which each technique is most useful and valid.

- Chapter 4 presents some local property determinations of Mo coating materials on steel, using another recently developed [14] method for property evaluation,

involving instrumented sharp indentation. A discussion of the technique and some experimental results are provided.

- Chapter 5 presents a summary of the conclusions from this work and presents suggestions for additional research topics to be considered in future work.

Chapter 2

Residual stress and property determination of graded coatings using a new curvature-based technique

2.1 Previous work

Coatings are used in a wide variety of practical applications, making their property and stress determination determination and a thorough understanding of their behavior very important. Knowledge of their properties and of processing-induced residual stresses prior to service is necessary, since a state of residual stress can alter the permissible design loadings and affect the mechanical performance and lifetime of the coatings.

In the past, a substantial amount of work has been performed to determine successfully the properties of thin film coatings, in particular for microelectronics applications. The stress state in a thin film (a film whose thickness is less than or equal to approximately one-hundredth of the substrate thickness) is simple to determine

from its curvature, using the Stoney formula [15] developed in 1909. This technique, commonly used in the microelectronics industry today, does not require a knowledge of the material properties of the coating, making the method very convenient to use, since the properties of thin films are often significantly different from the corresponding properties of the same material in its bulk form. Only the elastic properties of the substrate are needed to determine the stress in a thin film, and this information is more readily obtained when the substrate is a thick and relatively well-known material, such as a standard silicon wafer. However, when the thickness of a coating is greater than or equal to 1/100th of the substrate, the thin film analysis is no longer completely accurate, and knowledge of the coating properties is required; hence a different technique is needed to determine the stresses in these thick coatings.

A number of different approaches have been undertaken in the past to assess the intrinsic stresses produced by various deposition methods [12,13] in thick coatings, mostly of homogeneous compositions. These techniques include:

- Destructive methods which involve successive removal of the deposited layers and determination of the resultant changes in the strain or curvature of planar or cylindrical specimens [16-19].

- In-situ measurement of strain or curvature during thermal spray or epitaxial growth of thin films [20-27].

- X-ray or neutron diffraction to probe the changes in lattice constants, from which a measure of the internal stresses can be obtained [28-32].

- Optical fluorescence, in which piezo-spectroscopic effects are used to determine the internal stresses in optically transparent materials [33,34].

A major drawback of *a posteriori* stress assessment techniques, such as layer removal, is that mechanical procedures such as grinding or hole drilling to remove deposits can induce surface compressive stresses, thus altering the stresses that the

technique is designed to measure. In addition, mechanical grinding is more difficult to apply uniformly to a multi-component layer, since a softer phase will be preferentially removed during the polishing process compared to a harder phase in the material. Chemical material removal, by etching or electro-chemical polishing, can remove material without altering the stress state that is being measured, unlike mechanical material removal. However, because chemical polishing can cause preferential and non-uniform chemical attack in a multi-component, composite layer, this technique is useful mostly for homogeneous materials in which layers of uniform thickness are more readily removed. Experimental difficulties in performing *in-situ* measurements may interfere with processing in many cases. A new experimental device has recently been developed to allow the in-situ measurement of curvature during the deposition process [35]. However, the foregoing methods do not capture the redistribution of stresses through the thickness of the deposited layer during cooling from the processing temperature, and they do not isolate the quench stresses from the thermal stresses without additional experiments.

Diffraction studies are also commonly used in the analysis of the residual stresses in coating materials. X-ray diffraction, a common and experimentally simple technique, is limited by the depth of penetration into the surface of the coating by X-rays, which is typically on the order of only a few micrometers. Synchrotron x-ray radiation increases the depth of penetration of the x-rays into the thickness of the coatings, but is less readily available experimentally. Neutron diffraction allows a large depth of penetration into coatings, and can thus be used to study thicker coatings. However, in addition to being a fairly expensive experimental technique to implement, the neutron diffraction studies are limited in spatial resolution to approximately 0.5 mm, making profiles of residual stress in a mm-scale coating more difficult to measure precisely. Both X-ray and neutron diffraction measure local properties, so local plastic deformation as well as local variations in composition, especially in the case of graded coatings, can elevate the uncertainty in stress estimates.

In view of the shortcomings of the available experimental methods, process modeling is often used to quantitatively derive the evolution of internal stresses for specific deposition techniques. Most such models are predicated upon first-principle calculations of the mechanics and physics of layer formation [36-42]. The key assumptions which enter into the analyses have not been directly checked with systematic experiments in most cases, and the complexity of various technologically significant processing methods causes the compounding of errors due to various approximations and simplifications needed to model them. This makes the applicability of the analyses to actual processing situations more difficult to establish, and makes the models most useful for improving general understanding, though they are often not able to predict the behavior of actual technological systems.

A lack of understanding of the processing-induced stresses renders the initial "mechanical condition" of the layered material to be unknown, even before it enters service [6-8]. As a result, subsequent thermomechanical reliability and life prediction analyses are prone to significant errors. This situation is further compounded by the fact that the thermal and mechanical properties of the surface coatings remain largely unexplored. In the few specific applications where detailed attempts have been made to determine the elastic moduli, thermal expansion coefficients and thermal conductivity of coatings, additional complications have been identified:

- Layered coatings, produced by such commonly used methods as thermal spray, are markedly more compliant, less thermally conductive, more anisotropic, and more porous when compared to bulk materials of the same composition [36,43-45].

- The thermal and mechanical properties of the coatings can vary over the range of temperatures of practical interest.

- While there exists some prior work (e.g., [46-48]) on the experimental measurement of the mechanical properties and residual stresses of homogeneous

coatings, no standard methods of proven reliability are available to probe the properties of graded coatings.

- To our knowledge, no experimental studies of the evolution of internal stresses during the processing of functionally graded coatings had been previously reported in the literature, and no procedures had been thus far formulated for the systematic evaluation of such properties as in-plane Young's modulus or coefficient of thermal expansion in graded coatings.

The objective of the work summarized in this chapter was to determine the processing-induced stresses and thermal properties of layered and graded coatings in a model Ni-Al_2O_3 system, using new experimental and analytical tools developed for this purpose [49-50]. Experimental validation of this method is provided with the aid of systematic measurements of intrinsic or quenching stresses and coefficient of thermal expansion for thermally-sprayed Ni–Al_2O_3 coatings of spatially homogeneous and graded compositions. In addition, some experimental data have been obtained for the Young's modulus of the coating materials, and microstructural observations of the materials were made and are presented here.

2.2 Curvature during successive layer build-up: methodology

2.2.1 Experimental Determination of In-Plane Young's Modulus of Coatings

Consider a homogeneous, layered or compositionally graded substrate in the form of an elastic plate or beam, whose total thickness, h_0, and spatial variation of the in-plane Young's modulus, $E(z)$, through its thickness z, are known. The average Young's modulus $\bar{E}_0$, the position of the neutral axis, z_{N0}, and the beam stiffness, I_0,

for this material can then be computed in the following way.

$$\bar{E}_0 = \frac{1}{h_0}\int_0^{h_0} E(z)dz \tag{2.1}$$

$$z_{N0} = \frac{1}{h_0\bar{E}_0}\int_0^{h_0} zE(z)dz \tag{2.2}$$

$$I_0 = \int_0^{h_0} z^2E(z)dz - (z_{N0})^2h_0\bar{E}_0 \tag{2.3}$$

Here, z_{N0} is the location where the strain is equal to zero when a pure bending moment is applied to the specimen. In the thermo-mechanical loadings that arise during processing, this neutral axis location may not always have a zero strain (because of a uniform stretch or contraction), but its geometrical position is taken as the reference point for I throughout the analysis that follows. It should be noted here that I has the meaning of beam stiffness, and not the moment of inertia based on purely geometrical cross-sectional properties.

For the simple case of a homogeneous substrate, $\bar{E}_0$ is the isotropic Young's modulus of the substrate, $z_{N0} = h_0/2$, and the beam stiffness, $I_0 = \bar{E}_0h_0^3/12$. The biaxial beam stiffness, which is representative of the equal-biaxial deformation of plate specimens, can then be written as,

$$I_{\text{bi}} = \frac{I_0}{(1-\nu)} = \frac{\bar{E}_0}{(1-\nu)}\frac{h_0^3}{12}, \tag{2.4}$$

where ν is Poisson's ratio. A state of equal biaxial stress exists in the plate when the length and width of the plate are significantly higher than its thickness, which is the case for the specimens considered in this work. In general, the analysis given here can be applied either to plates or to beams, with the Young's modulus E for the case of a beam being replaced by the biaxial modulus $E/(1-\nu)$ for the case of a plate in a state of equal biaxial stress. In a small region confined to the free edges of the plate, over a distance of the order of the plate thickness, a multi-axial state of stress exists which, for the purposes of this study, can be neglected without much error, since all

of the measurements were performed away from the edges of the specimens. It is also worth noting here that only variations in E through the thickness of the coating and the substrate are considered here. The variation in ν is not taken into account.

Now consider the deposition, on the substrate, of a new layer of thickness Δh for which the Young's modulus is to be determined. The total thickness of the beam/plate now is $h_1 = h_0 + \Delta h$. This geometry is shown in Figure 2-1. The stiffness of the beam can be measured experimentally by evaluating the curvature, κ, of the beam upon the application of a constant bending moment, M, with, for example, four point bend loading. The new bending stiffness I_1 becomes

$$I_1 = \frac{M}{\kappa}. \tag{2.5}$$

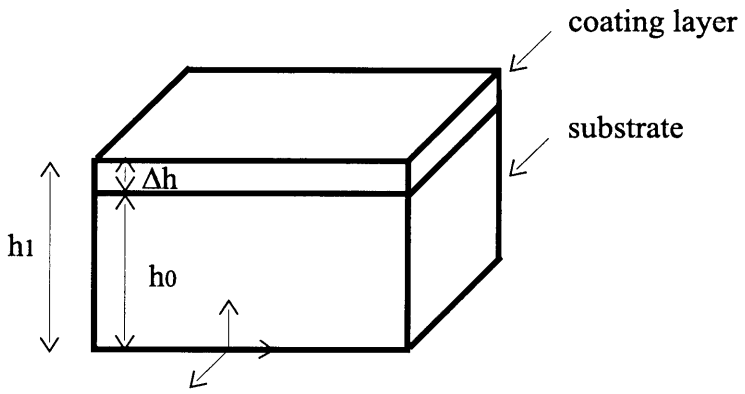

Figure 2-1: Geometry of a substrate with a single deposited layer and the associated dimensions

From the difference between the bending stiffness values, $\Delta I = I_1 - I_0$, it is possible to deduce the average in-plane Young's modulus E of the added layer of thickness Δh. The exact solution is given by elementary beam theory (e.g. [51, 52]) to be

$$E = \frac{-b + \sqrt{b^2 - 4ac}}{2a\Delta h} \tag{2.6}$$

where

$$a = \frac{\Delta h^2}{12}, \tag{2.7}$$

$$b = h_0\bar{E}_0[\frac{1}{3}(h_1^2 + h_1h_0 + h_0^2) - z_{N0}(h_1 + h_0) + z_{N0}^2] - \Delta I, \tag{2.8}$$

$$\text{and } c = -h_0\bar{E}_0\Delta I \tag{2.9}$$

In the thin film limit, where $\Delta h \ll h_0$,

$$E = \frac{\Delta I}{\Delta h} \cdot \left(h_0 - z_{N0} + \frac{\Delta h}{2}\right)^{-2}. \tag{2.10}$$

Once the Young's modulus of the added layer has been evaluated, the new average Young's modulus $\bar{E}_1$, moment of inertia, I_{bi1}, and the new position of the neutral axis, z_{N1}, of the beam of total thickness h_1 can be updated as follows:

$$\bar{E}_1 = \frac{\Delta hE + h_0\bar{E}_0}{h_1} \tag{2.11}$$

$$z_{N1} = \frac{h_0\bar{E}_0 z_{N0} + \Delta hE(h_0 + \frac{\Delta h}{2})}{h_1\bar{E}_1} \tag{2.12}$$

$$I_{\text{bi1}} = \frac{E\Delta h^3}{12} + E\Delta h\left(h_0 - z_{N1} + \frac{\Delta h}{2}\right)^2 + \frac{E_0h_0^3}{12} + E_0h_0(z_{N0} - z_{N1})^2 \tag{2.13}$$

If a second layer of thickness Δh is now deposited on the first layer such that the total thickness of the beam/plate becomes $h_2 = h_1 + \Delta h$, the in-plane Young's modulus of the second layer can be determined exactly in the same away (using the four-point bend loading method) as that described above for the first layer; the average modulus of the specimen with two layers and the new neutral axis position $\bar{E}_2$ and z_{N2} are then found. This procedure is then repeated for each subsequent layer.

In order to determine the in-plane Young's modulus of each layer as a function of temperature, the foregoing four-point bend experiment should be carried out on the specimen at different temperatures, and the analysis repeated for each temperature.

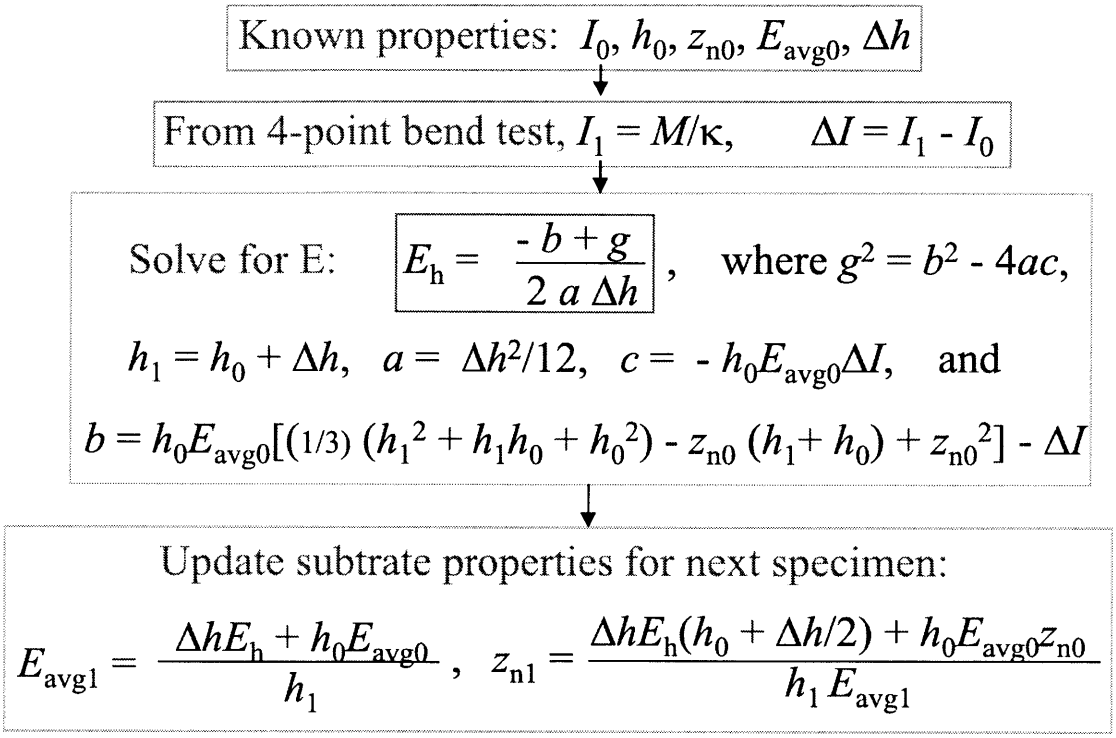

Figure 2-2: Flowchart showing procedure to calculate E of a coating layer

It is worth noting here that beam bending methods to assess the elastic properties of homogeneously layered materials have previously been reported (e.g., [46, 47]). The present work, however, for the first time extends this approach to graded coatings by recourse to deposition involving multiple specimens and layers.

The procedure described above is summarized in flowchart form in Figure 2-2.

2.2.2 Experimental determination of the coefficient of thermal expansion of coatings

Once the Young's modulus of the multi-layered material is known from the procedure outlined in the previous section, additional information on the average coefficient of thermal expansion (CTE) of each deposited layer, α, as a function of temperature and thickness position can be determined using simple thermal loading and curvature

measurements. In fact, these additional experiments can be carried out in conjunction with the bend tests using the same measurement techniques, if *in-situ* heating and cooling are feasible. If experimental capability exists for the measurement of curvature during heating and cooling, but *in-situ* four-point bend loading during curvature measurement is not feasible, the following procedure for CTE determination can still be carried out without the four-point bend tests. For this purpose, however, *a priori* estimates of the Young's modulus variation through the thickness of the multi-layer are needed from some other techniques or calculations (such as the rule-of-mixture estimate).

Consider a homogeneous, layered or compositionally graded substrate in the form of a plate or beam of total thickness h_0. The distribution of Young's modulus, $E(z)$, and coefficient of thermal expansion (CTE), $\alpha(z)$, through the thickness of the substrate are known. $\bar{E}_0$, z_{N0}, and I_0 are then computed from Eqs. 2.1– 2.3. The average CTE, $\bar{\alpha}_0$, and the gradient of substrate curvature with temperature, $d\kappa_0/dT$, are then computed, respectively, by

$$\bar{\alpha}_0 = \frac{1}{h_0 \bar{E}_0} \int_0^{h_0} E(z)\alpha(z)dz \tag{2.14}$$

$$\text{and} \quad \frac{d\kappa_0}{dT} = \frac{1}{I_0} \int_0^{h_0} (z - z_{N0})E(z)\alpha(z)dz. \tag{2.15}$$

For the simple case of a homogeneous substrate subject to a uniform temperature, $\bar{\alpha}_0$ is the CTE of the substrate, and $d\kappa_0/dT = 0$. It should be noted here that the above integrations assume that both E and α remain constant with temperature over the range from the deposition temperature to room temperature. (For the relatively small range of 130°C encountered in the present study, this is a reasonable assumption, and the experimental measurements of curvature versus temperature were in fact found to be very nearly linear.)

Now consider the deposition, on the substrate, of a new layer of thickness Δh for

which the CTE is to be determined, at any temperature, T. The total thickness of the plate now becomes $h_1 = h_0 + \Delta h$. In order to determine CTE at T, we subject the specimen of thickness h_1 to a small temperature change, ΔT, about a baseline temperature T, measure the corresponding change in the overall curvature, $\Delta\kappa_1$, to obtain

$$\frac{d\kappa_1}{dT} = \lim_{\Delta T \to 0} \frac{\Delta\kappa_1}{\Delta T}. \tag{2.16}$$

Define curvature variation $\Delta\kappa$ due to the temperature change ΔT about T as

$$\left[\frac{\Delta\kappa}{\Delta T}\right]_T = \frac{d\kappa_1}{dT} - \frac{d\kappa_0}{dT} \tag{2.17}$$

The average coefficient of thermal expansion, at temperature T, of the newly added layer of thickness Δh is then given by,

$$\alpha = \left[\frac{\Delta\sigma^o}{\Delta T}\right]_T \frac{1}{E} + \bar{\alpha}_0 \tag{2.18}$$

where

$$\left[\frac{\Delta\sigma^o}{\Delta T}\right]_T = I_1 \left[\frac{\Delta\kappa}{\Delta T}\right]_T \frac{1}{\Delta h}\left(h_0 - z_{N1} + \frac{\Delta h}{2}\right)^{-1}, \tag{2.19}$$

with I_1 and z_{N1} given by Eqs. 2.5 and 2.12, respectively. The average CTE of the beam of total thickness h_1, can now be updated as follows:

$$\bar{\alpha}_1 = \frac{h_0 \bar{E}_0 \bar{\alpha}_0 + \Delta h E \alpha}{\bar{E}_1 h_1} \tag{2.20}$$

where $\bar{E}_1$ is given by Eq. 2.11. The foregoing steps are repeated each time a new layer of homogeneous or graded composition is deposited.

A flowchart summary of the procedure described above can be found in Figure 2-3.

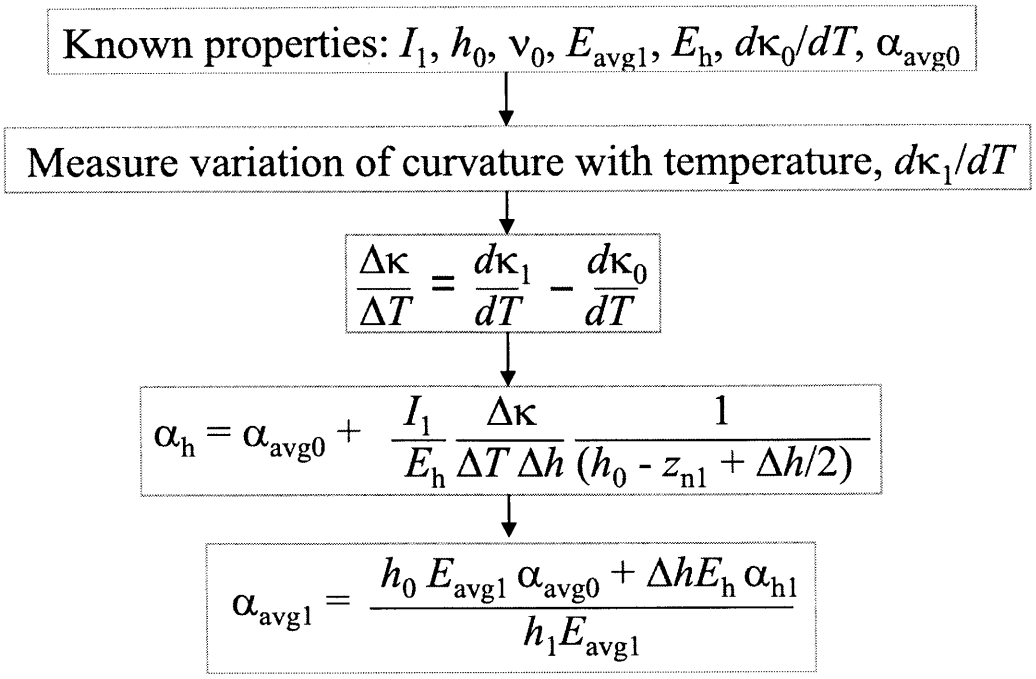

Figure 2-3: Flowchart showing procedure to calculate CTE of a coating layer

2.2.3 Determination of the residual stresses due to processing

As new layers of material are deposited on a bare substrate or substrate with previously deposited layers, the curvature of the overall deposit–substrate system changes, as does the stress in the deposited layer, and in the substrate, including any previously-deposited layers that form part of the substrate. This change in curvature and stress with deposition of new layers on a substrate is illustrated in Figure 2-4.

Knowledge of I_1, h_0, ν, z_{N1}, $\bar{E}_1$, and $E(z)$ is sufficient to compute the exact stress state in the new added layer. Here we assume that the inelastic strain resulting from processing in the added layer is uniform through the thickness of this new layer.

The curvature of the specimen has to be evaluated by experimental measurement before and after processing at a given temperature T. The variation of curvature, $\Delta\kappa$, is enough to provide internal stress distribution in the plate due to strain mismatch between substrate and the new added layer. The average stress in the added layer at

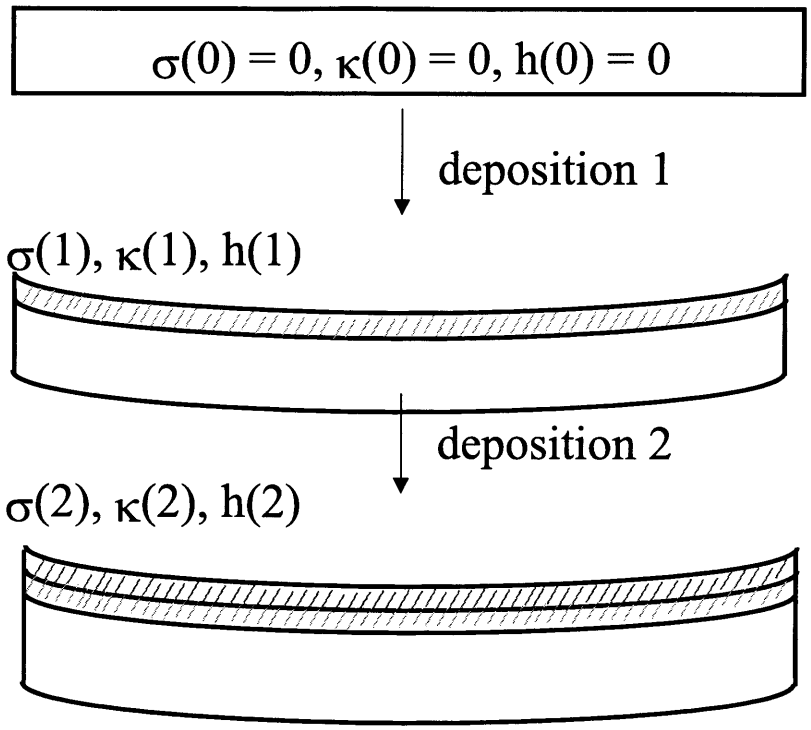

Figure 2-4: Schematic diagram of the change in stress and curvature resulting from deposition of new layers on a substrate

the temperature T is equal to

$$\sigma^T(z) = \sigma^\circ + E(z - z_{N1})\Delta\kappa - \frac{\Delta h E \sigma^o}{h_1 \bar{E}_1}, \tag{2.21}$$

where

$$\sigma^\circ = I_1 \frac{\Delta\kappa}{\Delta h} \frac{1}{(h_0 - z_{N1} + \frac{\Delta h}{2})}. \tag{2.22}$$

The strain mismatch in the added layer will also alter the stress state in the substrate. The variation of the stress in the substrate at the position through the thickness z due to the presence of the new added layer is equal to

$$\Delta\sigma^T(z) = E(z)(z - z_{N1})\Delta\kappa - \frac{\Delta h E(z) \sigma^o}{h_1 \bar{E}_1} \tag{2.23}$$

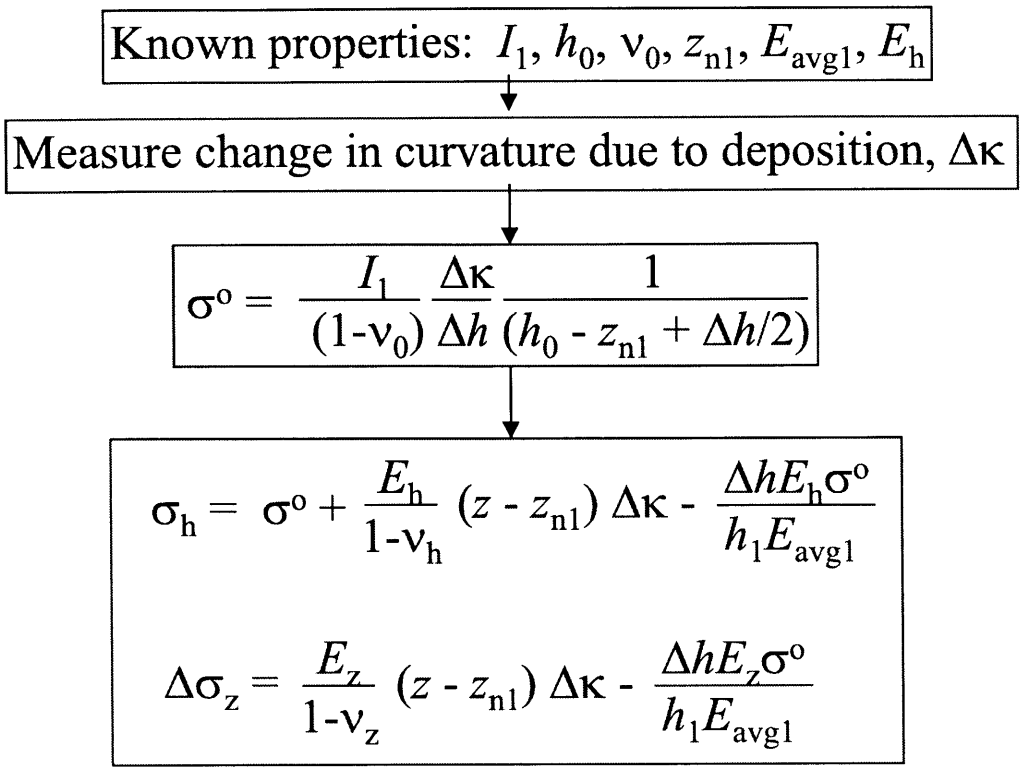

Figure 2-5: Flowchart showing procedure to calculate stress of a coating layer

where $E(z)$ is the Young's modulus at the position z.

The above-described procedure is summarized in flowchart form in Figure 2-5.

2.2.4 Scope and Limitations of the Work

The method used here enables the experimental determination of through-thickness variations in processing-induced stresses at room temperature, without altering the stress state during measurements, such as that occurring in mechanically invasive techniques such as layer removal and hole-drilling. The method also accounts for the thermal mismatch stresses induced by cooling from the processing temperature to room temperature, and isolates them from the intrinsic quenching stresses produced by the deposition process. The method also facilitates the determination of stresses, Young's modulus, and coefficient of thermal expansion as a function of position in

the coating, and also the variation of these properties as a function of temperature at any given position within the coating.

The present method, however, has some limitations. The experiments are performed on deposited layers of finite thicknesses, and the calculations determine the average Young's modulus, coefficient of thermal expansion, and processing-induced stress for each layer or sublayer. Thus, the resolution of the through-thickness property determination of the coatings is limited by the smallest layer thickness which can still produce accurate measurements of E and α that can be distinguished from the measurements of the substrate properties alone. Experimentally, it is difficult to produce a continuously graded material, and a large number of measurements (typically involving ten or more sublayers) needs to be made in order to obtain the highest possible accuracy. However, this makes the experimental measurements of Young's modulus more difficult to distinguish as the thickness of the layers decreases.

In addition, the process of interrupting the deposition to remove partially-coated specimens from the deposition chamber adds an intermediate cooling and heating step to the deposition procedure, which could theoretically alter the intrinsic stress distribution in layers. However, to minimize the effect of this problem, the substrates and partially-deposited specimens were all pre-heated to the deposition temperature experienced by the previous layer before the deposition of any additional layers was made on each specimen, and all of the substrates were pre-heated to the standard deposition temperature prior to the deposition of the first layers. In addition, because of the substantial size of each deposited layer spatially, it is likely that any remaining effect not countered by the pre-heating of the substrates would be most pronounced near the edges of each layer, and not near the middle of each deposit. Thus, since the technique presented here measures the average stress in each layer, it is unlikely that this effect would significantly alter the determination of the average residual stresses in each deposited layer. Simple modifications to the specimen holder in the deposition chamber could also be designed which facilitate the removal of a single

specimen (among a number of specimens) without any interruption in the deposition process.

The present method does not account for the variation in the Poisson ratio, ν, through the thickness of the coated layer, which can introduce some errors in the estimates of the biaxial moduli. However, since variations in ν span only a range of 0.26–0.32 for the materials considered in this work, the magnitude of any error introduced by not considering the variation of ν is not expected to be significant.

In addition, α was assumed to be constant with temperature over the limited temperature range from processing to room temperature. This approximation is a reasonable one given the very nearly linear experimental relation between curvature and temperature of the specimens studied here.

Finally, the analyses employed here for the interpretation of stresses and material properties are predicated upon linear elasticity theory. Consequently, they provide accurate measures of stresses and properties only when the deposition conditions and subsequent thermal and mechanical loading do not induce plastic flow in the coating and the substrate.

In the remainder of this section, the analytical framework of the new method is presented. The experimental details are presented in the following section.

2.3 Experimental Procedure and Materials

2.3.1 Substrate preparation

Substrates for deposition were prepared from an SAE 1010 cold-rolled steel sheet (nominal composition 0.1 wt% C), by cutting the specimens into 19.1 mm x 50.8 mm x 0.7 mm plates, and polishing one side to obtain a reflective surface for the curvature measurements. The initial substrate curvatures were recorded using a Tencor FLX-2900 laser scanning device (Tencor Instruments, Mountain View, CA).

2.3.2 Plasma-spray deposition

Plasma spray deposition was chosen as the procedure for producing the specimens studied. Plasma spray deposition is widely used in industry for the production of coatings for a wide variety of applications because it is a relatively inexpensive process with the flexibility to produce coatings of mixed or varying compositions. The procedure introduces residual stresses into coatings during their production, and it is advantages to understand the nature of these stresses that result from the deposition process. Thus coatings were produced by plasma-spray deposition for the study of processing-induced residual stresses summarized here.

Coatings were deposited on the steel substrate in an ambient atmosphere with an automated single-gun plasma-spray apparatus, shown schematically in Figure 2-6 (State University of New York at Stony Brook). Ni and Al_2O_3 powders were fed using two separate feeders, mixing the feed just prior to injection into the plasma spray torch, with the relative amounts of metal and ceramic adjusted in 5 percent increments to form a graded material beginning with Ni on the steel substrate and continuing in 5% increments to Al_2O_3 on the surface layer. For high concentrations of the ceramic ($\geq$ 60% Al_2O_3), the powders were pre-mixed prior to feeding to ensure sufficient mixing of the metal and ceramic. The substrates were preheated before each deposition to approximately 70°–100°C to obtain a relatively uniform temperature distribution during deposition. The substrate temperature during the deposition process, on the deposit side, was measured using an optical pyrometer, and was found to vary between 77°C and 158°C, with temperatures increasing gradually and cyclically throughout the deposition process. During the deposition, the plasma torch was rastered across an area with dimensions slightly larger than that of a single specimen to increase the uniformity of the deposit thickness. Six specimens at a time were held magnetically on a rotating carousel and were rotated past the plasma gun.

The resulting microstructure produced by the plasma-spray process consists of a layered microstructure with a high level of porosity consisting of disc-shaped "splats"

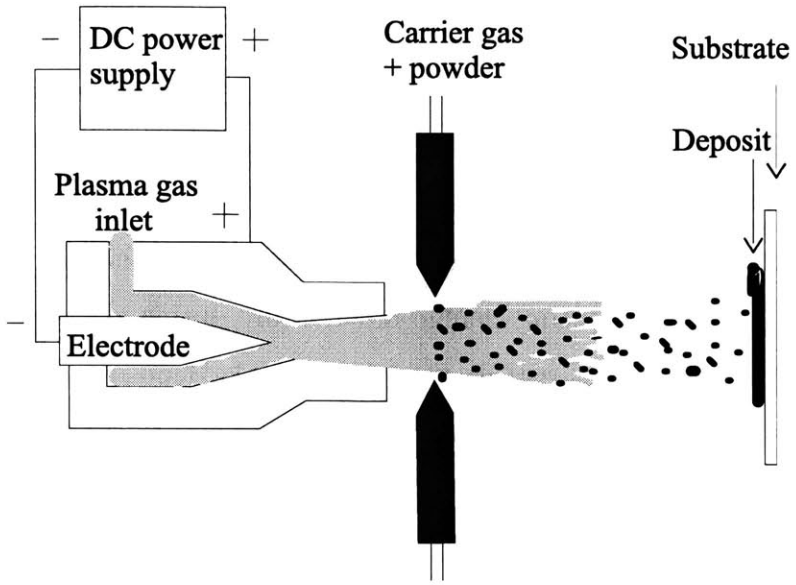

Figure 2-6: Schematic diagram of plasma spray apparatus used

of solidified material on the substrate. The splats typically have an approximate thickness of 5–15 μm and approximate in-plane dimension of about 20–175 μm. Between the splats, particularly within layers, typically exist large pores or microcracks, resulting in a coating with an overall porosity of 6-12%. A schematic illustration of a typical microstructure produced by a plasma spray deposition process is shown in Figure 2-7.

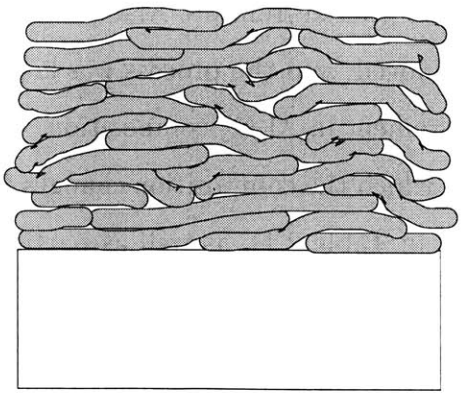

Figure 2-7: Schematic diagram of a typical microstructure produced by plasma spray deposition

The polished side of each substrate was protected with a cloth tape resistant to

high temperatures to preserve the reflective surfaces for future curvature measurements. In addition, several of the substrates were exposed to various grit-blasting treatments to obtain a measurement of the resulting curvature change in the substrate due to the surface treatment alone. Grit-blasting is often used to roughen the surface of a substrate prior to deposition to allow better adhesion between the deposit and the substrate. The resulting change in curvature during grit-blasting was found to be much higher than the curvature resulting from the deposition, making the latter difficult to discern accurately if superimposed on the former. Therefore, the graded material layers were deposited directly onto the unpolished surface of the substrates, with no further surface treatment such as grit blasting applied prior to deposition. Despite the absence of a surface preparation prior to deposition, good adhesion was found between substrate and coating for every specimen except for that in which pure Al_2O_3 was deposited directly onto the steel.

The deposition process was stopped at 20% composition increments. Six substrates were inserted into the plasma spray chamber and a first layer of Ni–5 wt% Al alloy was deposited onto each steel substrate under identical processing conditions. Then one specimen was removed from the chamber and replaced by a new substrate. The remainder of the specimens were then deposited, all under identical conditions, with a second layer that was graded from 0% Al_2O_3 to 20% Al_2O_3. One of the original specimens was then removed, and the process was continued with each deposited layer containing a 20% increment in Al_2O_3 composition. Single-layer specimens, each with a graded layer within which the composition changes from one end of the layer to the other (specimens 7–12 in Table 2.1), as well as partially-formed graded coatings (specimens 1–6 in Table 2.1) were prepared. The deposit thickness and substrate thicknesses are shown in Table 2.2.

A schematic representation of the deposition process showing the successive build-up of layers for the partially-graded and fully-graded specimens and the single graded layers deposited on the steel substrates is shown in Figure 2-8. The figure illustrates

#	Ni-5%Al	0-20% Al_2O_3	20-40% Al_2O_3	40-60% Al_2O_3	60-80% Al_2O_3	80-100 %Al_2O_3	100% Al_2O_3
1	X						
2	X	X					
3	X	X	X				
4	X	X	X	X			
5	X	X	X	X	X		
6	X	X	X	X	X	X	X
7		X					
8			X				
9				X			
10					X		
11						X	
12							X

Table 2.1: Compositions of Ni-Al_2O_3 FGM's

#	substrate thickness (mm)	deposit thickness (mm)
1	0.645	0.069
2	0.673	0.282
3	0.665	0.529
4	0.671	0.708
5	0.671	1.112
6	0.663	1.554
7	0.668	0.226
8	0.671	0.266
9	0.671	0.221
10	0.668	0.422
11	0.673	0.246
12	0.665	0.181

Table 2.2: Thicknesses of Ni-Al_2O_3 FGM's

the procedure for producing the single-layered and multiple-layered graded specimens.

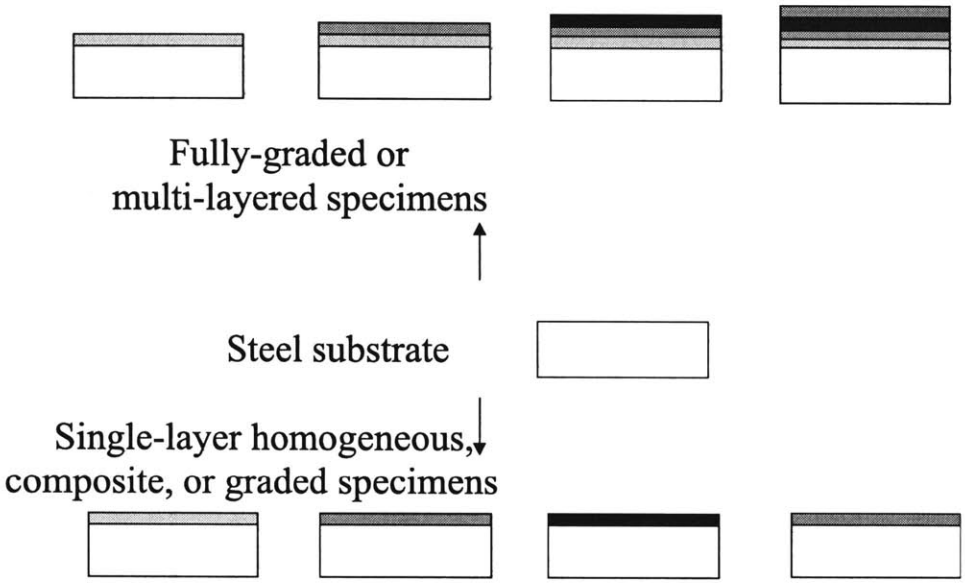

Figure 2-8: Schematic diagram of specimen preparation by successive build-up of layers

2.3.3 Curvature measurements

The final curvature of each specimen was measured after deposition, and the initial curvature was subtracted to obtain the change in curvature due to the deposition process. In addition, each of the first batch of specimens was heated at 4°C/min to 100°C, held for one hour to allow an equilibrium steady state temperature to be reached, heated to 150°C, held for one hour again, and then cooled to room temperature to determine the change in curvature with temperature. The curvature measurements were performed on the Tencor FLX-2900 (Tencor Instruments, Mountain View, CA) laser scanning system. The curvature versus temperature data were used to determine the CTE and the intrinsic and residual stresses in the materials. A schematic diagram of the curvature measurement apparatus is shown in Figure 2-9.

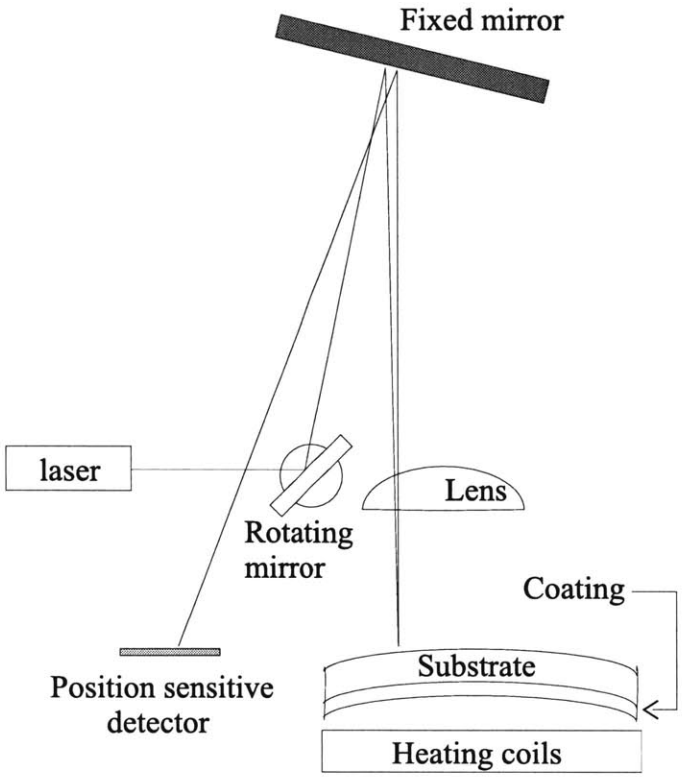

Figure 2-9: Schematic diagram of curvature measurement apparatus

2.3.4 Four–point bend tests

After measurements of post-deposition curvature at room temperature and curvature variation with temperature change, each of the specimens was then cut lengthwise using a Buehler Isomet 2000 precision saw, and two of the specimens, a bare steel substrate and the full FGM, were subjected to a four-point bending load in an Instron 4200 mechanical testing apparatus (Instron Corporation, Canton, MA), with the deflection of the specimens measured by crosshead displacement. The values of Young's modulus of the specimens were subsequently determined using the analysis given previously to compare with the predictions of Young's modulus resulting from a rule-of-mixtures calculation.

In addition, four–point bend tests were performed on each of the cut specimens using a four–point bending apparatus in an Instron 85215 mechanical testing machine

(Instron Corporation, Canton, MA), and the results used for low-resolution thick-layer property evaluation of the specimens. The four–point bending apparatus is shown schematically in Figure 2-10.

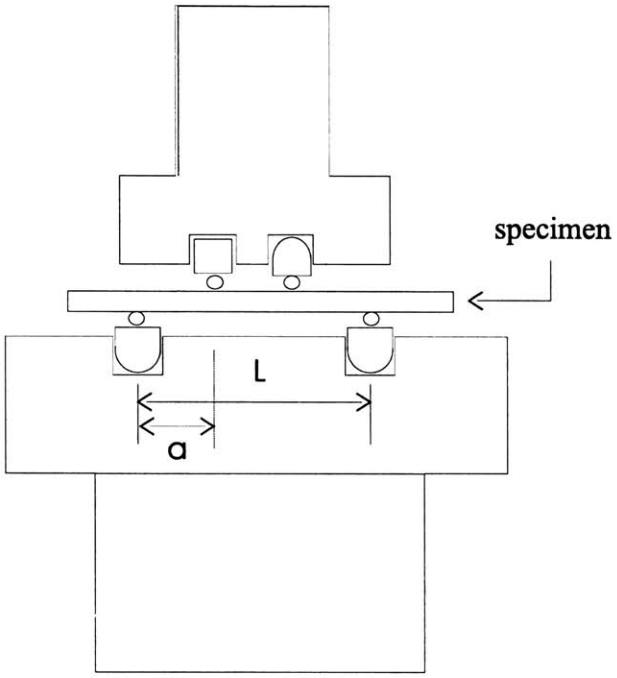

Figure 2-10: Experimental set-up for four–point bending tests

2.3.5 Microstructural evaluation

The microstructures of the specimens were examined using optical microscopy, scanning electron microscopy (SEM), and computed tomography (CT) scans. After all curvature measurements were made on each specimen, the specimens were sectioned, polished on a cross-section, and examined in both an optical microscope and in an SEM. A section of the fully-graded specimen was also examined using a CT scan on a Computed Tomography system with a Feinfocus FXE-200.50 X-ray system and an OIS 904 X-ray detector system (Linköping University, Linköping, Sweden). For this purpose, in-plane sections of the FGM were examined at 20 evenly-spaced intervals across the cross-section. The plasma-sprayed microstructures and defects were

examined using all three techniques.

2.4 Results and discussion

2.4.1 Coating microstructures

Figure 2-11 shows the microstructure of a fully–graded deposit on steel ranging from Ni at the bottom to pure Al_2O_3 at the top. At higher magnification (Figure 2-12), the microstructure of the deposited materials can be seen more clearly, with wavy individual splats of Ni and Al_2O_3 intermixed randomly, along with some porosity (in the range 6–12 volume per cent). As the composition of Al_2O_3 increases, the corresponding increase in the concentration of the Al_2O_3 splats is evident as the darker regions in Figure 2-12.

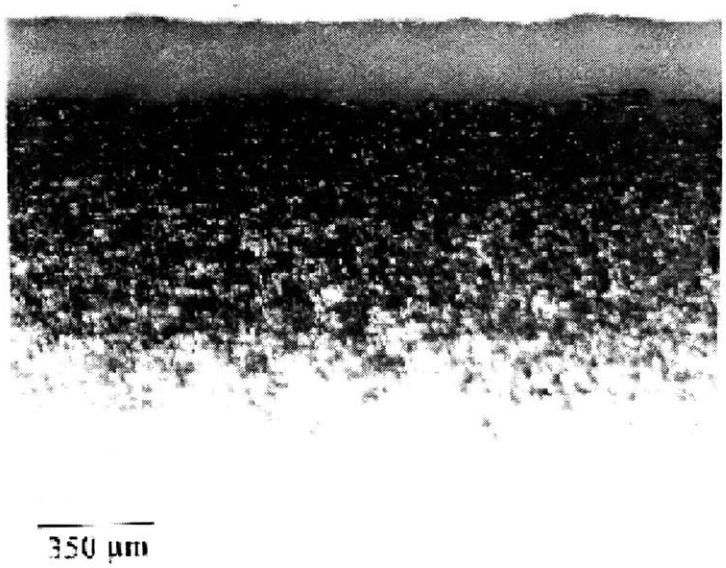

Figure 2-11: Microstructure of Ni–Al_2O_3 FGM

The CT scans were used to search for internal defects within the microstructure that were not visible in the external cross-section. The resolution of the CT scans is approximately 5-10 micrometers, which is larger than the typical size of pores and microcracks resulting from the plasma spray deposition process. Thus, only defects

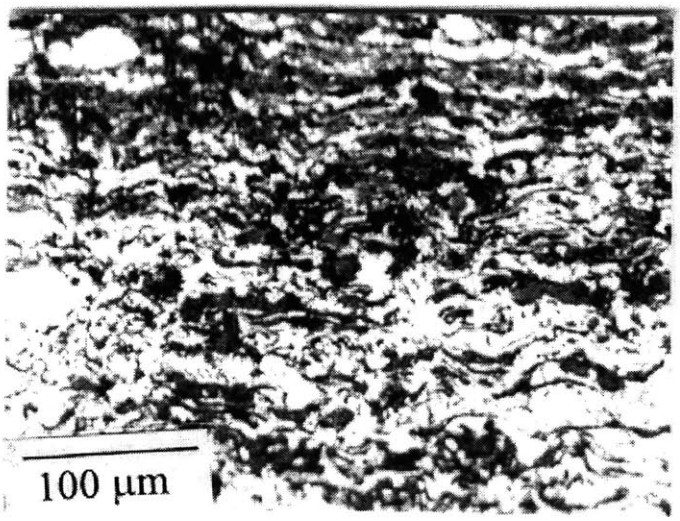

Figure 2-12: Microstructure of Ni–Al_2O_3 FGM at higher magnification, showing the wavy nature of layered deposits formed by plasma spraying. Ni is the lighter area, and Al_2O_3 is the dark area.

larger than these common micro-scale defects from the deposition process can be detected using the CT scanning technique. It was found by the CT scans that the FGM specimen studied did not contain any larger-scale cracks or defects that were visible within the resolution of the CT scanning apparatus.

2.4.2 Residual stresses and thermo-mechanical properties of the coatings

The two types of specimens, i.e., the single-layered graded specimens on steel substrates and the multiple-layered FGM specimens, were each examined using the methodology outlined above. The values of isotropic Young's modulus E and coefficient of thermal expansion α at room temperature that were used in the calculations for the steel substrate and the bulk constituent phases of the coatings, i.e., Ni-5%Al and Al_2O_3, are listed in Table 2.3. In the temperature range 20°C to 150°C (i.e., the temperature range of cooling from the deposition temperature), the coefficients of

	E (MPa)	α ($10^{-6\circ}C^{-1}$
Ni-5%Al	207	12
Al_2O_3	380	5.4
1010 steel	207	12

Table 2.3: Properties of the constituent phases of the graded coatings and substrate

thermal expansion were found to be approximately independent of the temperature, and the Young's moduli of the materials were assumed to be independent of temperature over this small temperature range. The average Poisson ratio, ν, of the coating was taken to be constant through the thickness, with a value of 0.32.

Single-layered specimens

The average stress in a single layer of a thin coating deposited on a steel substrate was calculated using the curvature change of the material during processing, the bulk properties of the steel substrate, the thickness of the substrate and the deposited layer, and the coefficient of thermal expansion and Young's modulus of the coating layer. One such monolayer specimen consisted of a single layer of nickel deposited on the steel substrate. The remaining layers were graded in 20% increments of Al_2O_3 composition, with one layer ranging from 0 to 20% Al_2O_3 in nickel, and the others ranging from 20–40%, 40–60%, 60–80%, and 80–100% Al_2O_3 in nickel (see Table 2.1). The biaxial stiffness of the beam substrates, I_{bi}, was calculated using the height, h_0, of the substrate, and the Young's modulus E and Poisson's ratio ν of the steel substrate.

The separation of the intrinsic quenching stresses due to the rapid solidification of the deposited splats onto the substrate from the thermal mismatch stress caused by the cooling of the fully-deposited specimens to room temperature from the deposition temperature were performed in order to separate the effects of the two main components contributing to the overall residual stress in the specimens at room tem-

perature. This separation of stress components was performed by calculating the coefficient of thermal expansion of each average layer of the deposit from the curvature versus temperature data obtained by the thermal cycling experiments. Two types of calculations were performed on the same specimens, one using a rule-of-mixtures calculation for the Young's moduli of the deposited layers, and one using experimentally determined values of the Young's moduli of the full specimens, with a low resolution, in combination with the rule-of-mixtures calculations for each thin deposited layer. A comparison was also made between the results obtained using the methodology presented here and the results that would be obtained using a thin-film approximation to calculate the stresses. The main advantage of the thin-film approximation method is that the average stress in the coating can be determined without the need for any measurement of the mechanical properties of the coating, provided that the thickness of the coating is significantly smaller that of the substrate. However, this approximation is not valid for many of the specimens considered here.

When the stiffness of the substrate is used to calculate the average stress in the deposited layer, using the thin-film approximation that the properties of the beam are dominated by the properties of the thick steel substrate, then the neutral axis of the beam, defined as the location where the strain is equal to zero when a pure mechanical bending moment is applied to the specimen, is located at $z_N = h_0/2$. Here, $\Delta\kappa$ is the change in curvature from a substrate with no deposit to a substrate with a coating layer deposited on it, Δh is the change in thickness from a substrate to a substrate with a coating layer, and h_0 is the substrate thickness. The classical Stoney formula for thin films [15], which was suitably modified for the present case, was used to determine the average stress in a single layer, graded coating:

$$\sigma = -\frac{I_{\text{bi}}\Delta\kappa}{(h_0 - z_N)\Delta h}. \tag{2.24}$$

Determination of Young's moduli In order to properly estimate the values of Young's modulus of the thin coating layers which enter into the calculations of α and residual stresses, it is necessary to have proper experimental measurements of the in-plane Young's moduli.

Using the Instron 85215 four-point bending set-up, plots of load, P, versus displacement, v, were made for each of the specimens. One such curve is shown in Figure 2-13.

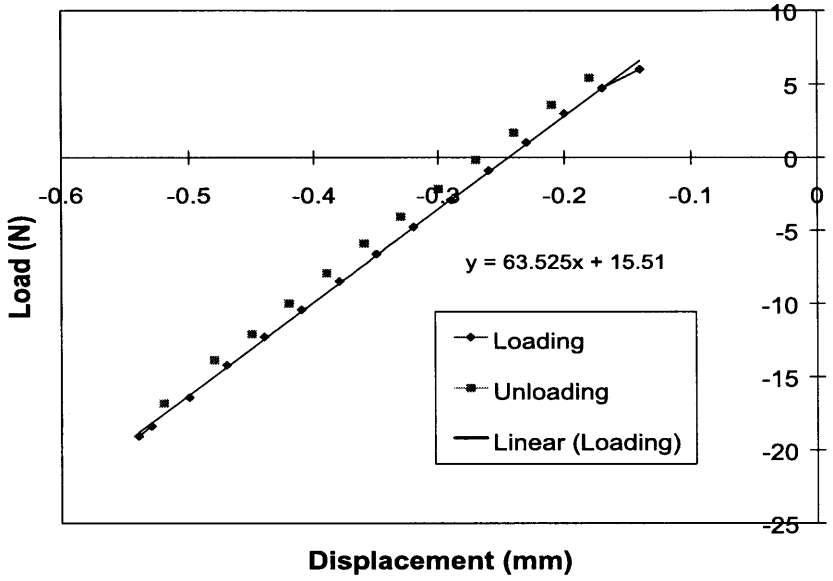

Figure 2-13: Plot of load versus displacement from 4-point bending test

From these curves, the slope, S, was used to calculate the Young's modulus, E, using the following equation:

$$E = \frac{KS}{bh^3}, \tag{2.25}$$

where b and h are the width and height of the specimen, respectively, S is the slope, and K is a constant that depends on the geometry of the four-point bend set-up. K is given by the following expression:

$$K = 2(3a^2L - 4a^3), \tag{2.26}$$

where L is the span of the outer supports in the four-point bend apparatus, and a is the distance between the outer and inner support on the same side.

The values for the entire substrate+coating stiffness were obtained in this manner, but the resolution of the testing technique used did not allow an accurate determination of the values of Young's modulus for just the thin layers of coating material, as the small thickness of these layers did not allow a distinction in the load-displacement curves calculated. Thus, the stress profiles calculated using the four-point bending data use the data for the full substrate + coating systems, and a rule-of-mixtures calculation (described below) for the thin coating layers.

In our experimental measurements of compliance changes for the steel substrate and for the fully-graded specimen during the application of a constant bending moment using the Instron 4200 four-point bend set-up, the average Young's modulus for the specimen with fully graded coating (Specimen #6 in Table 2.1) was determined to be 54 GPa. A steel substrate tested alone was found to have a Young's modulus of 193 GPa using the same experimental set-up. This value is significantly smaller than the bulk Young's modulus of Ni and Al_2O_3, which are 207 GPa and 380 GPa, respectively (see Table 2.3). Thus the plasma-sprayed porous coatings used in our present study have been found to be significantly more compliant than the fully dense bulk specimens comprising the same constituent phases. This result is fully consistent with other studies (e.g., Pajares et al. [53], Hillery et al. [54], Suresh et al. [55], McPherson [56], and Sturlese et al. [57]).

On the basis of this information, we have consistently chosen the values of Young's modulus for the constituent Ni and Al_2O_3 phases to be one-fifth of their respective bulk material values, for subsequent analyses. While there are likely to be small differences in the levels of porosity between the Ni-rich and alumina-rich end of the graded layer, the extent of porosity at either end was independently estimated to be in the range 8–12%. These rule-of-mixture calculations of Young's modulus are used for the stresses presented in this and future chapters.

Determination of thermal expansion coefficients The average coefficient of thermal expansion of each graded coating deposited on a steel substrate was determined for the above specimens, using the change in curvature with temperature of each specimen as determined by the thermal loading experiments. Each experimental loading and unloading experiment resulted in a plot of curvature versus temperature for the specimens. A typical curvature versus temperature plot is shown in Figure 2-14.

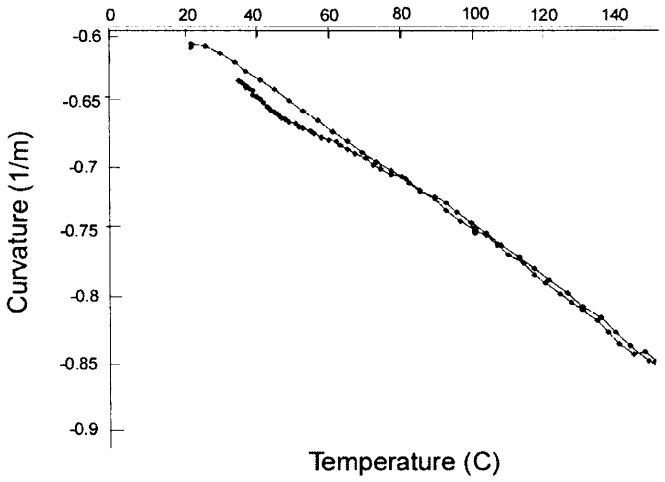

Figure 2-14: Plot of curvature versus temperature from thermal cycling experiment

For the purpose of estimating the CTE values of the composite coatings of Ni and Al_2O_3 shown in Table 2.1, Young's modulus was estimated by using the rule of mixtures as described in the previous section, with the average value of Young's modulus for each layer being proportional to the values of Young's modulus of plasma-sprayed Ni and Al_2O_3 (i.e., one-fifth of the bulk modulus value), in proportion to their composition by volume in each specimen. The experimental curvature versus temperature data from the thermal loading experiments were used to calculate the CTE, along with the rule-of-mixtures estimates of E, modified to account for the porosity of plasma-sprayed deposits.

The results of these calculations are presented in Figure 2-15, in which average coefficient of thermal expansion of each added layer is plotted versus average volume %

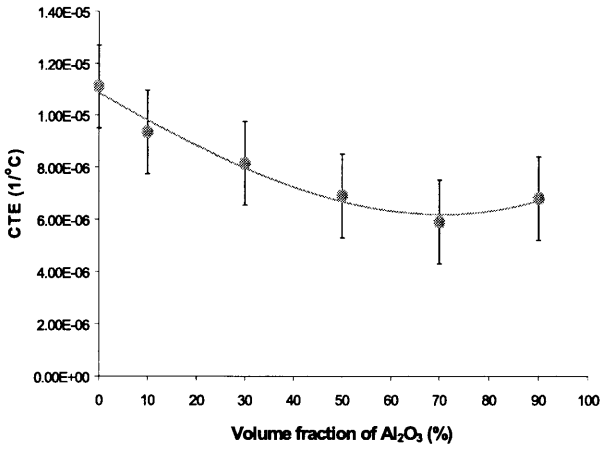

Figure 2-15: Plot of CTE vs. composition in Ni–Al_2O_3 specimens

Al_2O_3 in each layer. The values of CTE decrease with increasing Al_2O_3 composition, with a slight increase in value at the Al_2O_3–rich end. This behavior can be best understood by examining the CTE behavior of a continuous-fiber composite in the directions parallel and perpendicular to the fiber directions, as shown in the bottom and top curves, respectively, in Figure 2-16. It can be seen from the behavior of the CTE in composite materials that the behavior exhibited by the graded coatings in this experiment lies intermediate between the two behaviors displayed in Figure 2-16, with our coatings exhibiting more characteristics of the CTE dependence along the fiber direction than perpendicular to it. This is to be expected, given that the deposited microstructures, while consisting of wavy and irregular splats, still were predominantly oriented in one plane; i.e., on the plane parallel to the substrate (see Figure 2-12, for example). Thus the coefficient of thermal expansion of our graded coatings exhibits characteristics intermediate between that of the two orientations of continuous fiber composites, demonstrating that the plasma spray-deposited specimens lie somewhere between the two extremes of composite behavior given in Figure 2-16.

Determination of residual stresses The estimated average value of total internal stress at 20°C calculated from the thin-film approximation in each of the single

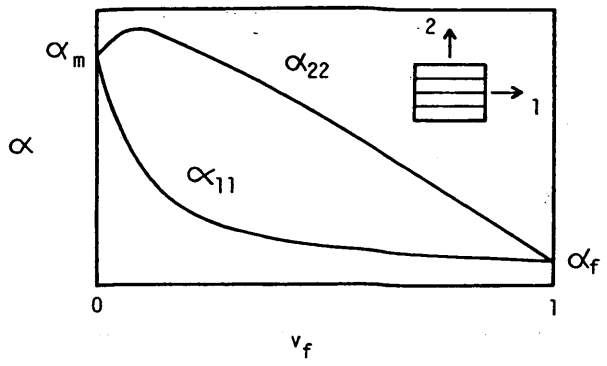

Figure 2-16: Coefficient of thermal expansion behavior of continuous fiber-reinforced composites [58].

graded deposits is plotted in Figure 2-17, as a function of the average Al_2O_3 content. The maximum tensile internal stress is recorded for the Ni-5%Al layer on the steel substrate with 0% Al_2O_3. For the graded single-layer coatings, Figure 2-17 shows the stresses corresponding to the average composition of the coating (e.g., for the 40–60% Al_2O_3 coating, specimen 9 in Table 2.1, the stress is plotted at an average Al_2O_3 concentration of 50% in Figure 2-17). With an increase in Al_2O_3 content, the tensile internal stress decreases. For the single coating with the highest Al_2O_3 content (i.e. for the 80–100% Al_2O_3), the average stress becomes slightly compressive. This qualitative trend in the stress profile is similar to that seen for the total residual stress at room temperature found using the plate formulation, as shown in the same Figure 2-17. However, the absolute values of the stresses are somewhat different, illustrating that the thin film approximation is not truly appropriate for the relatively thick coatings studied here.

The residual stresses at room temperature in graded single-layer deposits calculated using the properties of the coatings are shown in Figure 2-17. In addition, the calculated CTE values were used along with the estimates of Young's modulus to determine the thermal mismatch stresses created upon cooling the graded materials from the processing temperature of 150°C to room temperature. From the difference between total residual stress at room temperature and the thermal mismatch stresses,

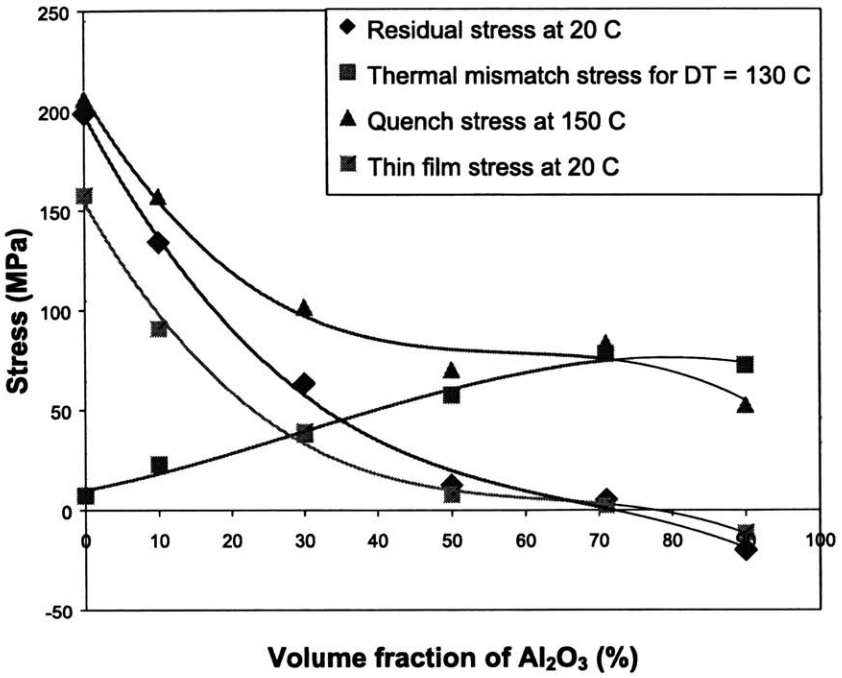

Figure 2-17: Stresses in single graded layers of Ni–Al_2O_3, using a rule of mixtures calculation for the Young's modulus

the intrinsic quenching stresses due to rapid solidification at the processing temperature were also determined. The total room temperature residual stresses, intrinsic quenching stresses at the processing temperature, and thermal mismatch stress for a temperature increase of 130°C are all shown in Figure 2-17. The values for the total residual stresses at room temperature differ by about 30–35% from the values given by the thin-film calculations based on the modified Stoney formula. This indicates that the thin-film approximation is not strictly valid for the thick-layered deposits studied here, thus making the analytical method necessary for an accurate stress determination. It is also worth mentioning that the stresses in the Ni layer were measured to be near 200 MPa, a value that is within the upper end of the published range of Ni yield stress. The values for Ni yield stress in the literature range from 140–200 MPa. In the material used in our studies, the yield stress seems to be near 200 MPa, the maximum stress reached in the Ni layers. Since the analytical method presented here depends on linear elastic beam and plate theories, it does not accurately capture the

behavior in places where local yielding has occurred. When plasticity occurs, in fact, the stress is likely to remain near this yielding stress rather than increasing in an elastic manner, such that the calculated solutions will probably overpredict the stresses in the yielded area of the pure metal and metal-rich graded area, which remain lower than their elastically predicted values.

The values of room temperature residual stress, thermal mismatch stress for a temperature increase of 130°C, and intrinsic quenching stress at the deposition temperature of 150°C for the same single-layered graded specimens discussed above are shown in Figure 2-18, using the 4-point bending test results for the large-scale values of Young's modulus of the full specimens and the rule of mixtures calculations for the Young's modulus of the thin coating layers.

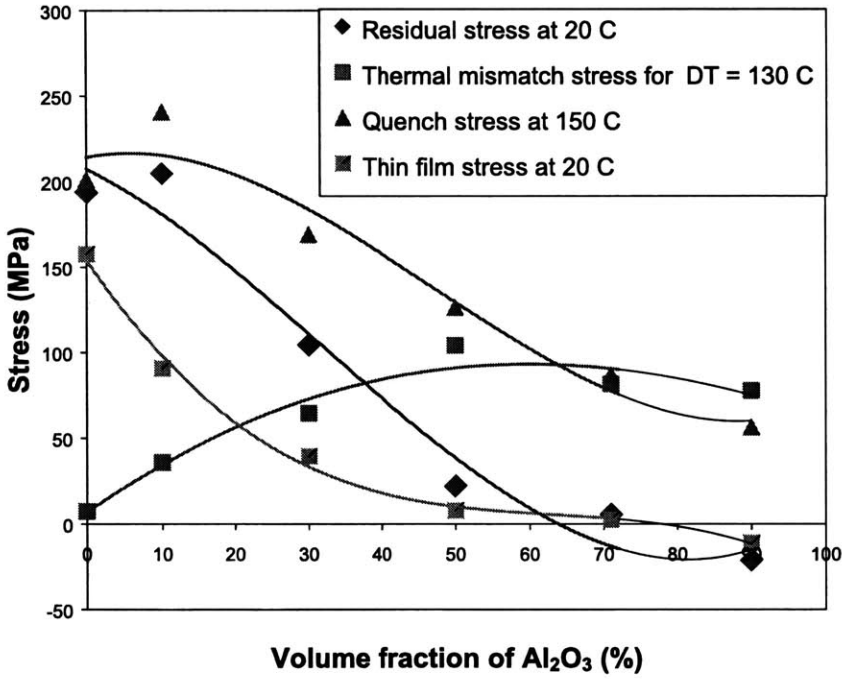

Figure 2-18: Stresses in single graded layers of Ni–Al_2O_3, usinga rule of mixtures calculation and 4-point bend test data to determine the Young's modulus

A comparison of Figures 2-18 and 2-17 shows that the values obtained using the two different methods for Young's modulus calculation are similar.

No direct comparison with prior work is possible for the graded coatings because

the present work constitutes the first experimental estimation of intrinsic stresses in metal-ceramic coatings with gradients in composition. For homogeneous coatings, the results shown in Figure 2-17 and 2-18 exhibit trends similar to other studies of residual stresses in plasma-sprayed deposits. Kuroda [23], for example, found tensile quenching stresses of approximately 140 MPa for Ni-20Cr on steel and lower stresses of about 30 MPa for plasma-sprayed Al_2O_3 on steel at deposition temperatures ranging from 60-100°C, while Kuroda and Clyne [37] found similar trends of positive quenching stresses on the order of 300 MPa for Ni and lower but still positive quenching stresses of 80–$\sim$100 MPa for Al_2O_3, at elevated processing temperatures of 400–1000°C. Howard and Clyne [26] studied deposition of a boron carbide ceramic on a Ti alloy substrate, and found compressive residual stresses in the ceramic deposit, ranging from about –130 MPa to 0 MPa. These trends are all consistent with the results found in the graded materials studied here, when comparing the ceramic-rich graded layers with the ceramic coatings, and the metal-rich graded layers with the metallic coatings.

The experimental results obtained in this work were also compared with an analytical formulation for residual stresses in materials, which is presented in [40]. Kroupa's formulation [40], which is briefly summarized below, models the intrinsic quenching stresses within the material as thermal mismatch stresses resulting from the cooling of a deposited splat from a stress-free temperature to the deposition temperature of the substrate.

In this formulation, the stress in the i-th layer of a deposit after the deposition of a total of n layers is given by the expression

$$\sigma_{i,n} = E_{bi}[(\sum_{k=i}^{n} A_k)z + \sum_{k=i}^{n} B_k - \alpha_i(T_s - T_i)], \tag{2.27}$$

where T_s is the bulk deposit temperature, T_i is the temperature at which the residual stresses start to develop in the i-th layer, and A_k and B_k are properties of the k-th layer, given by the following equations.

$$A_k = \frac{(F_k M_k - S_k N_k)}{(F_k I_k - S_k^2)}, \tag{2.28}$$

$$B_k = \frac{(I_k N_k - S_k M_k)}{(F_k I_k - S_k^2)}, \tag{2.29}$$

$$F_k = \sum_{i=1}^{k} E_{bi} h_i, \tag{2.30}$$

$$S_k = \frac{1}{2} \sum_{i=1}^{k} E_{bi} (z_i^2 - z_{i-1}^2), \tag{2.31}$$

$$I_k = \frac{1}{3} \sum_{i=1}^{k} E_{bi} (z_i^3 - z_{i-1}^3), \tag{2.32}$$

$$N_k = E_{bi} h_k \epsilon_k, \tag{2.33}$$

$$M_k = \frac{1}{2} E_{bi} (z_k^2 - z_{k-1}^2) \epsilon_k, \text{and} \tag{2.34}$$

$$\epsilon_k = \alpha_k (T_s - T_k). \tag{2.35}$$

The actual values of stress obtained from this analytical formulation depend significantly on the temperature that is assumed to be a stress-free temperature for the solidification of the coating materials. Kroupa reports that experimental studies have found that the stress-free temperature of Al_2O_3 solidifying onto a substrate during plasma spray deposition is approximately 1000°C. In comparing his formulation with the experimental results obtained here, stress-free temperatures were chosen to enter into the model based on the choice of temperature that results in the same endpoint stress for each of the pure phases. These temperatures were found to be 355°C for Ni and 1166°C for Ni–Al_2O_3.

The stresses resulting from the entire coating cooling from these temperatures are shown in Figure 2-19, along with the experimental quenching stress at 150°C. In addition, a volume-averaged temperature intermediate between these two phases is plotted for the case where the endpoints are matched to the experimental data, and for the case where the stress-free temperature is matched to the experimental data for Ni, while the stress-free temperature chosen for the Al_2O_3 phase is as reported by

Kroupa. It can be seen that while the analytical model can partially capture some of the trends of the solidification, it does not provide a fully accurate or complete picture of the variation of the quenching stresses as a function of the change in composition of the coating layers. This is in part because the quenching stress includes other factors in addition to the constrained contraction upon solidification, such as non-equilibrium cooling, thermal gradients, and possible annealing affects on lower deposit layers due to deposition of newer layers on top of them.

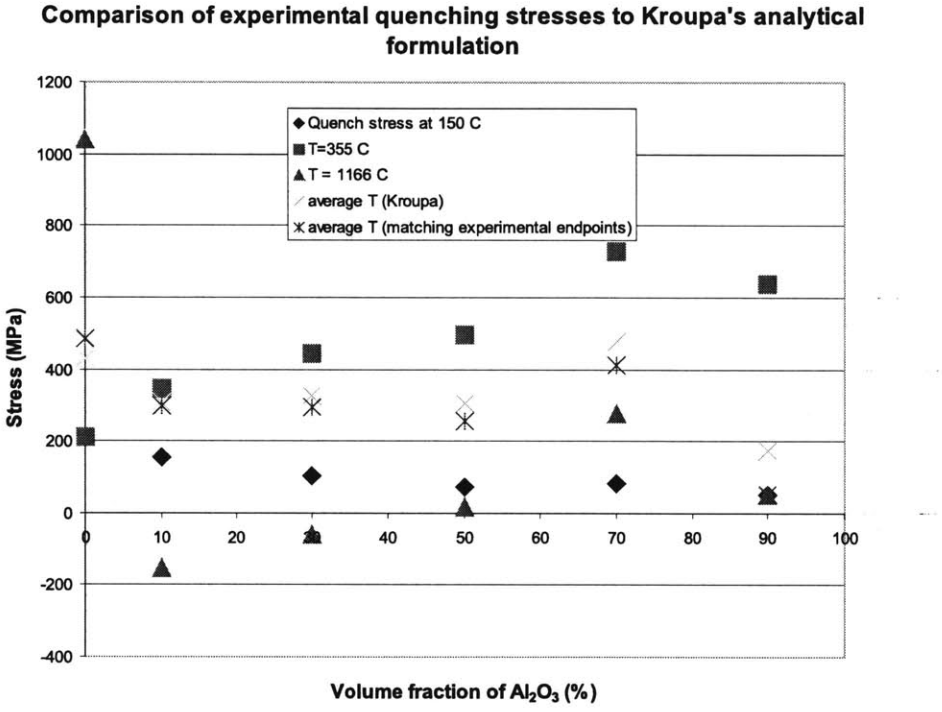

Figure 2-19: Comparison of experimentally determined quenching stresses at 150°C in single graded layers of Ni–Al_2O_3 with an analytical model of quenching stresses presented in [40]

Multi-layered graded deposits

The residual stress through the thickness of a fully graded layer ranging from Ni to Al_2O_3 was also calculated, both with the rule of mixtures calculations of Young's

modulus, and with the combined experimental and rule of mixtures calculations, as described in the previous section. The specimens used for this determination consisted of steel substrates on which a metal layer (Ni) was deposited, followed by graded layers of mixed Ni–Al_2O_3 composition with deposition stopping after a composition of 0%, 20%, 40%, 60%, 80%, and 100% Al_2O_3 was reached (specimens 1-6 in Table 2.1). Curvature and thickness measurements of each specimen before and after deposition were performed. The differences in thickness and curvature from one specimen to a consecutive one with an additional graded 20% compositional increment were taken as the deposit thickness and associated curvature change, respectively, for each layer with that same compositional variation throughout the six specimens. This assumption of one specimen with n layers acting as the substrate in calculations for the properties of a specimen with $n+1$ layers introduces an additional source of experimental error over and above that found in the calculations performed on thin graded layers in the previous section. However, it also allows the change in residual stress in a layer due to the subsequent layers deposited on top of it to be determined, thus allowing the residual stress profile through the thickness of a fully-graded deposit to be calculated. The residual stress in a fully-graded Ni–Al_2O_3 FGM is shown in Figure 2-20. The steel substrate remains in a state of compressive residual stress, while the stress in the deposited layers is predominantly tensile. The stress increases with increasing purity of the deposit, and decreases in the central range of mixed compositions. The highest value of tensile residual stress is attained at the surface of the Al_2O_3 deposit, where it reaches a value of nearly 200 MPa. Figure 2-20 shows the residual stresses at room temperature that would result in a layer at each position through the thickness if no additional layers were deposited on top of it, and also the total stress in each layer as a function of position through the thickness. It can be seen from these plots that the deposition of additional layers on top of previous layers induces a small change toward slightly more compressive stresses in the layers below it, as the tensile quenching stresses develop in the newly-deposited layer (see, e.g., Figure 2-17).

The values of these small shifts in stress with deposition of additional top layers are also shown in the figure. These values are each slightly compressive. The thermal mismatch stresses between the deposit and the substrate are not high enough to compensate for the tensile quenching stress in each newly-deposited layer, so that the effect of each such layer on the layers below is to induce a net compressive change in the stress relative to the stress that would result in each layer if no additional layers were deposited on top of it.

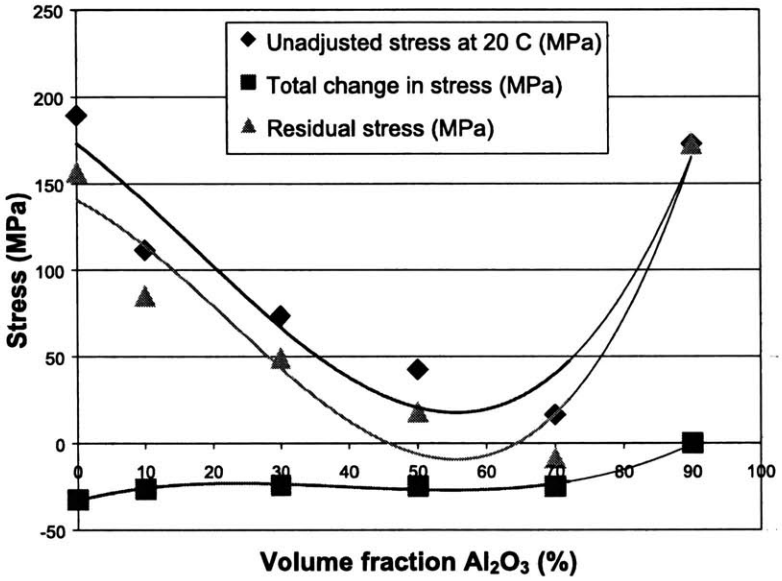

Figure 2-20: Through-thickness stresses in a fully-graded Ni–Al_2O_3 specimen, using a rule of mixtures calculation to determine Young's modulus

Figure 2-21 shows the same plot of through-thickness stress in a fully-graded Ni–Al_2O_3 specimen, with the bending data from the four-point bend experiments used for the Young's modulus calculations of the thick specimens in conjunction with rule-of-mixtures calculations for the Young's modulus of each thin coating layer. As seen before for the single-layered graded specimens, the values obtained using the two methods are comparable.

The maximum tensile stress in the surface layer comprising 100% Al_2O_3 of approximately 200 MPa is near the tensile strength of bulk (fully-dense) Al_2O_3 ($\sim$ 200–250

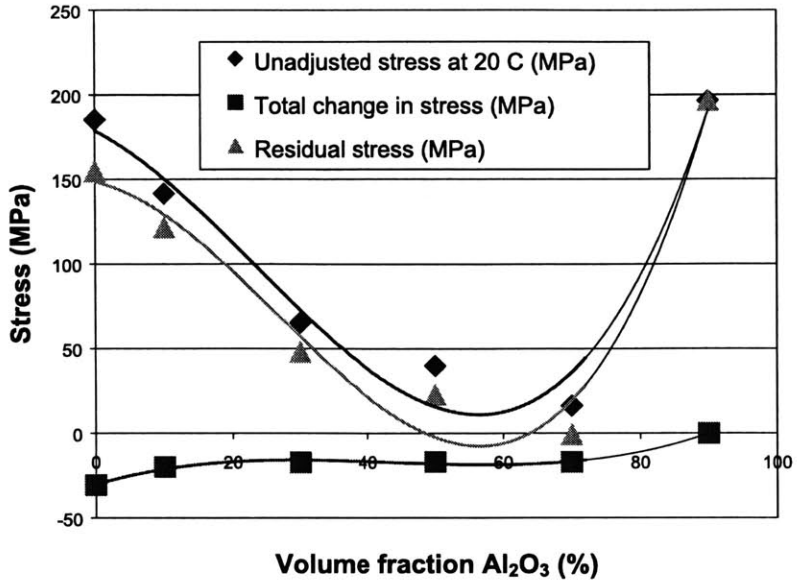

Figure 2-21: Through-thickness stresses in a fully-graded Ni–Al_2O_3 specimen, using a rule of mixtures calculation and 4-point bending data to determine Young's modulus

MPa). Since the plasma sprayed deposits have a high level of porosity, one would expect them to have a lower fracture strength than that of the bulk material, and thus one could expect cracks to develop in some of the plasma-sprayed coatings with the plane of the crack oriented perpendicularly to the surface (i.e. the cracks would be expected to advance in the direction of compositional gradients) under the biaxial stress state. This was indeed observed. Figure 2-22 shows an optical micrograph of a crack advancing in the direction of increasing Ni content through the fully-graded deposit, after a sectioning cut was made through the specimen to examine the microstructure.

2.5 Conclusions

To allow the stress and property determination of thick, inhomogeneous coating materials, an experimental method has been developed to determine the residual stresses at room temperature, the intrinsic stresses at the processing temperature resulting from the deposition process, and the coefficient of thermal expansion and Young's modulus of a layered or graded material as a function of depth in the deposit. This

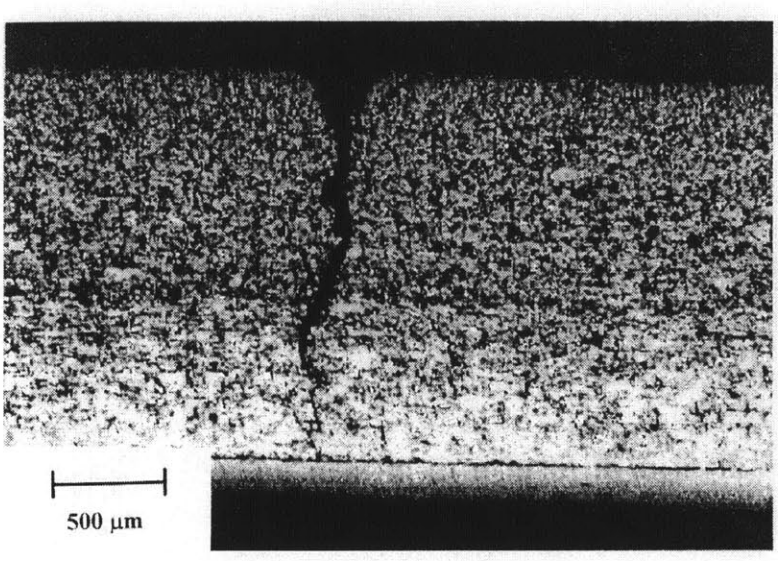

Figure 2-22: Microstructure of fully-graded Ni–Al_2O_3 specimen, showing growth of a crack in a direction perpendicular to the coating layers.

method has been successfully utilized to determine the residual stresses and thermal expansion coefficient in functionally graded Ni-Al_2O_3 layers deposited on a steel substrate by plasma spray deposition. The method can also, in principle, be used to determine physical and mechanical properties of layered and graded coatings produced by a number of different processing methods, including physical vapor deposition. It is found when Ni–Al_2O_3 composite coatings, typically 180-420 μm thickness, are plasma-sprayed onto a thick steel substrate, residual stresses as large as 200 MPa are found in the coating at room temperature. For the fully graded coatings, where the coating is sprayed in 7 discrete steps, the tensile residual stresses in the coating are largest at the Ni-rich and Al_2O_3-rich ends, and decrease in the central portion of the coatings where the composition is more evenly mixed. The maximum tensile residual stress of nearly 200 MPa occurs in the Al_2O_3 surface layer. The values of in-plane Young's modulus of the graded coatings have been measured to be as low as 54 GPa. Such low E values are found to be consistent with other independent estimates of the elastic properties of plasma-sprayed materials. The CTE values of

the Ni–Al_2O_3 composite coatings deposited by thermal spray are also assessed using the curvature measurement technique, and are found to be comparable to the values of the bulk properties.

Chapter 3

Stress determination in graded and homogeneous metallic, ceramic, and composite coatings

3.1 Introduction

Plasma spraying is a widely used technique for the production of various protective coatings which find applications as thermal-barrier, wear-resistant, and corrosion-resistant surface layers. These coatings are made from a broad range of materials encompassing metals, ceramics and polymers. The process involves introduction of the material, in the form of powder, to a plasma flame, which melts the particles and propels them towards the substrate to be coated. Upon impact, the particles flatten, cool down and solidify, forming a solid layer. As a result of this process, the coatings have properties quite different from bulk materials of the same composition, as a consequence of porosity, anisotropy, and residual stress.

Residual stresses in plasma sprayed coatings originate from the large temperature differences experienced during the deposition process. When the molten particles strike the substrate, they are rapidly quenched, while their contraction is constrained

by their adherence to the substrate. This leads to tensile stress in the coating, commonly referred to as quenching stress. During the deposition, the substrate is usually at some elevated temperature; during post-deposition cooling to room temperature, thermal mismatch stress develops due to the difference in thermal expansion between the coating and the substrate. Quenching and thermal mismatch stresses are the two main contributions to the overall residual stress. High residual stresses can lead to cracking, spallation of the coating, shape changes, etc. and in general can undermine the performance of the entire part. Thus, knowledge of the stress state is necessary to understand its evolution, assess its impact on the lifetime and function of the coated part, and to enable the control of the stress by modification of the manufacturing process.

Thus, the work presented in this chapter was undertaken with the objective of analyzing a variety of coating material systems produced by plasma spray processing, in order to better understand the behavior of such coating materials.

There are several commonly used methods of stress determination in coatings: mathematical modeling (analytical or numerical), material removal techniques (hole drilling, layer removal), mechanical methods (curvature, displacement, or strain measurement), and diffraction (X-ray or neutron) methods. Each technique has certain advantages and limitations [13,50]; their applicability is determined by such factors as shape, dimensions, materials of the coating and the substrate, knowledge of the constituents' properties and processing conditions, and also the availability of the necessary equipment. This chapter utilizes diffraction and curvature measurements in order to determine the stresses in FGM and homogeneous coatings. Some of the advantages of neutron diffraction include its non-destructive nature, ability to determine stress in each individual phase of a composite, and applicability to specimens of various sizes and shapes. X-ray diffraction was used as a complementary technique; it can determine stress only in a thin surface layer, whereas the penetrating power of neutrons enables through-thickness stress profiling without any material removal.

The curvature method allows determination of stresses in thick layers of graded or inhomogeneous composition, and is non-destructive. This method has a narrower spatial resolution than the neutron diffraction technique, and thus allows more detailed and precise through-thickness stress profiling of deposited layers, as presented here. However, unlike the neutron diffraction technique, the curvature method can be used on only simple geometries of specimens, like the ones studied here.

Three material systems were studied: single-material metallic coatings of Mo and 2 types of metal-ceramic composite coatings: Ni–Al_2O_3 and NiCrAlY–ZrO_2, where the ZrO_2 is stabilized with yttria (yttria-stabilized zirconia or YSZ). Molybdenum coatings find applications mainly in the automotive industry, on surfaces where low friction and high wear resistance are required [59]. The study of molybdenum coatings has focused on the effects of thickness on residual stress in the coating and the substrate as well. The results from all three techniques will be presented here, as average stresses in coatings of different thickness, as well as a through-thickness stress profile in the full coating.

The NiCrAlY+YSZ system is the most common material combination used for thermal barrier coatings in jet engines, diesel engines and power generation systems. A model system consisting of Ni+ Al_2O_3 and the industrially important NiCrAlY+YSZ were both investigated. The typical thermal barrier coatings consist of simply two layers - the ceramic topcoat and the metallic bondcoat. The sharp interface between the two layers, however, is generally the most frequent site of failure. This has led to the investigation of graded coatings [5, 60–65], with composition continuously varying from pure metal to pure ceramic, in order to make the interface more diffused, thereby reducing the stress discontinuity in the coating. This study has concentrated on residual stress as a function of thickness in homogeneous composite layers of fixed composition, as well as residual stress as a function of composition in graded coatings. The techniques used allow the separation of the quenching and thermal stress in the total stress, and the stress contribution of each phase to the

Powder	Composition (wt%)
Mo	Mo
Ni	Ni+ 5Al
Al_2O_3	Al_2O_3
NiCrAlY	Ni + 16.5Cr + 5.5Al + 0.5Y
YSZ	ZrO_2+ 8 Y_2O_3

Table 3.1: Compositions of the feedstock powders

total average layer stress. The results from diffraction and curvature measurements are compared and their specific significance and limitations highlighted.

3.2 Experimental details

3.2.1 Specimen characteristics

Three material systems were chosen for use in this study: Mo, Ni+Al_2O_3 , and NiCrAlY+YSZ composite coatings on steel substrates. Mo coatings were chosen due to their usefulness in automotive applications, while NiCrAlY+YSZ coatings were chosen due to their applications in diesel and jet engines and power generation systems, while Ni+Al_2O_3 coatings were chosen due to their usefulness as a model ceramic+metal graded coating system which is fairly easy to manufacture due to the mutual insolubility of the two component materials. All specimens were produced by atmospheric plasma spraying using a PlasmaTechnik PT-F4 torch (Sulzer-Metco Inc., Westbury, NY) (see Figure 2-6). The compositions of the feedstock powders, in weight percentages, are summarized in Table 3.1.

The deposition procedure described in Chapter 2 was used in the preparation of the specimens. The substrates were mounted on a rotating carousel, with the plasma torch moving vertically across the substrates. The substrates were preheated before deposition by plasma flame alone and air-cooled during deposition, in order to achieve

uniform deposition temperature (approximately 150°C). For the study of molybdenum coatings, a set of six specimens was prepared on 0.67 mm thick substrates with the coating thicknesses varying from 0.1 to 1 mm. All were produced at the same time; different thicknesses were attained by periodic removal of the sprayed specimens from the spraying chamber during a pause in deposition. These specimens were used in both curvature and diffraction measurements. For the study of composite coatings, separate sets of specimens were produced for the curvature and diffraction experiments. For the curvature measurements, FGM (functionally graded material) NiCrAlY+YSZ coatings ranging from 0.1 to 1 mm, and FGM Ni+ Al_2O_3 coatings ranging from 0.07 mm to 1.6 mm in thickness were deposited on steel substrates of thickness 0.67 mm. For all of the graded NiCrAlY+YSZ coatings, the compositions started at 100% metal adjacent to the substrate, and were graded in a direction perpendicular to the substrate to varying degrees of ceramic mixed with the metal, as shown in Table 3.2. For graded Ni+Al_2O_3 coatings, the first specimen consisted of a nickel coating on a steel substrate. The remaining specimens were graded, with each specimen consisting of a substrate and a deposited layer containing approximately a 20 volume percent increment of composition from a more metal-rich composite to a more ceramic-rich composite. The proportion of ceramic in each composite increased in the direction away from the substrate. The ranges of composition for each specimen, determined by x-ray diffraction, are shown in Table 3.3. Different compositions were achieved by feeding the powders with two separate feeders and varying feed rates, while mixing the powders just before injection to the flame. For high ceramic content, the powders were pre-mixed prior to feeding, to ensure uniform mixing. For the neutron diffraction measurements, 2-mm thick coatings were deposited on 2.5-mm thick substrates. For the two composite combinations, a set of 5 different fixed compositions was deposited onto 5 different substrates. The compositions of the specimens studied by neutron diffraction are also summarized in Table 3.3.

	Composition (vol % of ceramic)					
Specimen #	0	0-56	56-74	74-85	85-97	100
1	X	X				
2	X	X	X			
3	X	X	X	X		
4	X	X	X	X	X	
5	X					X

Table 3.2: Composition, in volume % ceramic, of the thick functionally graded NiCrAlY-ZrO_2 coatings used for curvature measurements. The table illustrates the successive build-up of graded layers during deposition by periodic removal of specimens. Each specimen contains each indicated layer with the given composition range.

NiCrAlY–ZrO_2: diffraction	Ni–Al_2O_3 : diffraction	Ni–Al_2O_3 : curvature
0	0	0
65	57	0–38
82	79	38-66
87	86	66-86
100	100	86-96
		96-100

Table 3.3: Composition, in volume % ceramic, of the single-layered composite coatings

3.2.2 Experimental procedure

Curvature method

Residual stress determinations were made by calculating the change in curvature of the specimens before and after deposition of successive layers. The procedure is the same as that described in detail in Chapter 2 and in [50,67]. A set of substrates was polished on one side and the initial curvature and thickness were measured. Coatings were then deposited on the unpolished surface, according to the compositions shown in Table 3.2, and the curvature and thickness after deposition were measured, using a Tencor FLX-2908 laser scanning device (Tencor Instruments, Mountain View, CA). The average stress in individual coating layers, as well as the change in stress within deposited layers due to the deposition of additional layers on top of previous ones, were calculated from these experimental results. The average stress, $\sigma(z)$, in a coating layer at position z through the thickness is given by equation 2.21:

$$\sigma^T(z) = \sigma^\circ + E(z - z_{N1})\Delta\kappa - \frac{\Delta h E \sigma^o}{h_1 \bar{E}_1}, \tag{3.1}$$

Here, E is the biaxial modulus for plate specimens or the Young's modulus for beam specimens, z is the position through the thickness of the specimen with the back of the substrate as the origin, z_{N1} is the position of the plane in the specimen (i.e. the neutral axis) where zero strain would occur when a pure mechanical bending moment is applied perpendicular to the z axis, $\Delta\kappa$ is the change in curvature due to the deposition process, Δh is the thickness of the deposited layer, h_1 and $\bar{E}_1$ are the new thickness and composite biaxial Young's modulus, respectively, after the deposition of a new layer onto the substrate, and σ° is the quantity defined in equation 2.22:

$$\sigma^\circ = I_1 \frac{\Delta\kappa}{\Delta h} \frac{1}{(h_0 - z_{N1} + \frac{\Delta h}{2})}. \tag{3.2}$$

Here, I_1 is the moment of inertia of the composite specimen after deposition has occurred. The quantity σ° is defined as a convenient collection of variables that is

used multiple times in the remaining calculations.

In addition, the through-thickness profile values of coefficient of thermal expansion (α) of the Ni–Al_2O_3 composites were calculated by measuring the change in curvature of the specimens due to thermal cycling from room temperature to the deposition temperature. The values of α were then used to isolate the intrinsic quenching stresses, due to rapid solidification upon deposition, from the subsequent thermal mismatch stress upon cooling to ambient temperature from the deposition temperature, as discussed in Chapter 2. The curvature change $\Delta\kappa$ due to a temperature change ΔT is used to calculate the average CTE, α, of a newly deposited layer based on the average CTE of the substrate, α_0, as in equation 2.23:

$$\Delta\sigma^T(z) = E(z)(z - z_{N1})\Delta\kappa - \frac{\Delta h E(z)\sigma^o}{h_1 \bar{E}_1} \tag{3.3}$$

In these calculations, the value of E_{bi} for a deposited layer is calculated using the linear rule of mixtures, with the endpoint values of E_{bi} taken as typical values of biaxial Young's modulus found in the literature for plasma-sprayed coatings, i.e., one-fifth of the bulk material modulus [53–57], as discussed in more detail in Chapter 2. The values of residual stresses calculated from the curvature measurements and thermal cycling experiments were compared to those from the neutron and X-ray diffraction measurements.

Diffraction methods

Stress determination by means of X-ray or neutron diffraction is based on measurements of changes in crystal lattice spacing, which manifest themselves as shifts in angular positions of respective diffraction peaks [68,69]. From a set of lattice spacings in different orientations and a stress-free lattice spacing, an elastic strain tensor is constructed, which is then converted to a stress tensor using Hooke's law. Generally, at least six measurements in different orientations are necessary for the determination of all six independent stress tensor components. Specimen geometry and physical

state may allow application of some assumptions that can reduce the number of necessary measurements. For example, if the specimen is thin in one direction, one can assume the stress in that direction to be zero. This stress state is characteristic of the typical equi-biaxial stress state in a layer away from free edges. In the present stress calculation, the assumption of zero stress perpendicular to the coating plane was used (for single-material coatings).

The X-ray diffraction stress measurements were performed on a Siemens D500 (Siemens AG, Karlsruhe, Germany) ω-diffractometer with Cu radiation (wavelength = 0.15405 nm), using the $\sin^2\psi$ method [70]. The stress at each point was determined from measurements in ten orientations ranging from -60 to 60 degrees from the specimen surface normal.

The neutron diffraction experiments were performed on the stress diffractometer at the National Institute for Standards and Technology (NIST), Gaithersburg, MD [71]. From a polychromatic beam of neutrons, a desired wavelength was selected by diffraction from a monochromator crystal (the wavelength being defined by the crystal lattice spacing and diffraction angle). The monochromatic beam illuminating the specimen was diffracted and detected by a position sensitive detector. Two apertures, one before and one after the specimen defined the size of incident and diffracted beams. Their intersection defined the "gauge volume" - the volume being probed by the neutrons. A gauge volume of 5 x 5 x 5 mm^3 was used in most cases, centered over the material of interest (coating, substrate), in order to eliminate the partial illumination effects. In some cases, when the stress gradient through the coating thickness was of interest and the coating had sufficient thickness, this volume was reduced to 0.5 x 0.5 x 7 mm^3. In the first case, average stress values from the entire coating thickness were obtained; in the second case, a through-thickness stress profile could be determined (see Figure 3-1). Two different orientations were used for one stress data point– in the plane and perpendicular to the plane of the coating – assuming an equal biaxial stress state. Thus, the in-plane stress was calculated

by comparing the in-plane strain to the strain perpendicular to the plane, under the assumption of zero stress perpendicular to the plane of the deposited layers. Where possible, more crystal reflections were used and the corresponding results were averaged. However, this approach was limited by the need to avoid overlapping of peaks from different phases present in the gauge volume (coating + substrate, metal + ceramic in the composite), and from multiple wavelengths incident on the specimen. Strains were converted to stresses using hkl-specific elastic constants, calculated from single-crystal constants [72] using the Eshelby-Kroener model [73]. The crystal planes used and the corresponding elastic constants (Young's modulus, E, and Poisson's ratio, ν) are summarized in Table 3.4.

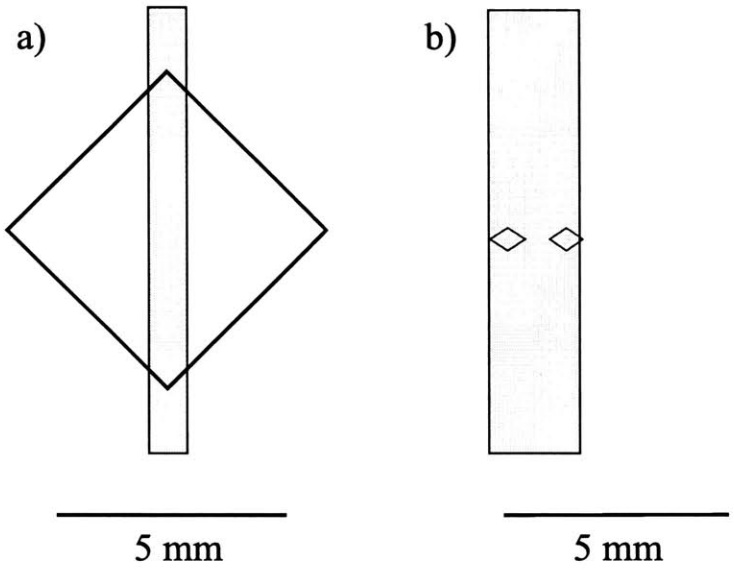

Figure 3-1: Schematic of the neutron diffraction measurement configuration for a) thin and b) thick coatings [74]. The diamond represents the gauge volume (intersection of the incident and diffracted beams), the gray area the diffracting material of interest. In the first case, the stress obtained is an average value from the entire layer; in the second case, a through-thickness stress profile can be obtained, with stress values averaged only from the small gauge volume at each position (2 such positions are marked by diamonds on figure b). The horizontal direction is the direction of coating thickness.

Composition of the composites was determined by X-ray diffraction, using the external standard method [75]. Reference samples were prepared by mixing known

Material	(hkl)	E (GPa)	ν
X-rays			
Mo	(321)	313	0.31
Neutrons			
Mo	(220)	313	0.31
Fe	(200)	170	0.33
	(211)	216	0.28
Ni	(111)	233	0.29
	(220)	215	0.31
	(311)	198	0.32
NiCrAlY	(200)	189	0.32
	(220)	216	0.29
Al2O3	(400)	250	0.26
	(440)	250	0.26
YSZ	(311)	200	0.30

Table 3.4: Details of the diffraction stress measurement and calculation: Miller indices of the crystal planes used for measurement, respective Young's moduli, and Poisson's ratios

amounts of the feedstock powders, and the dependence of relative intensity of the diffraction peaks on volume fraction was determined for each material. Using this dependence, the composites' phase compositions were determined from comparison of peak intensities of the composite and pure coatings.

3.3 Results and discussion

3.3.1 Molybdenum coatings

The effect of coating thickness on residual stress in plasma sprayed Mo coatings on steel was studied, and the results are presented below. Figure 3-2 shows the surface stress, as measured by X-ray diffraction, in Mo coatings of varying thickness on steel substrates. The thickness plotted is the total thickness of a layer of Mo on steel, and the stress plotted is the surface stress in the coating deposited up to

that thickness. The stress in the thinnest layer is relatively high (approximately 100 MPa); for higher thicknesses it retains a roughly constant value (about 40 MPa). Tensile stress in the surface layer is a result of quenching of the impinging splat; as it cools down, its shrinkage is restricted by adherence to the substrate and the splat is brought into tension [74]. In the present case, the tensile quenching stress is at least partially retained, although the thermal mismatch stress, developed upon cooling from deposition to ambient temperature is compressive (since the coefficient of thermal expansion/contraction of molybdenum is lower than that of steel).

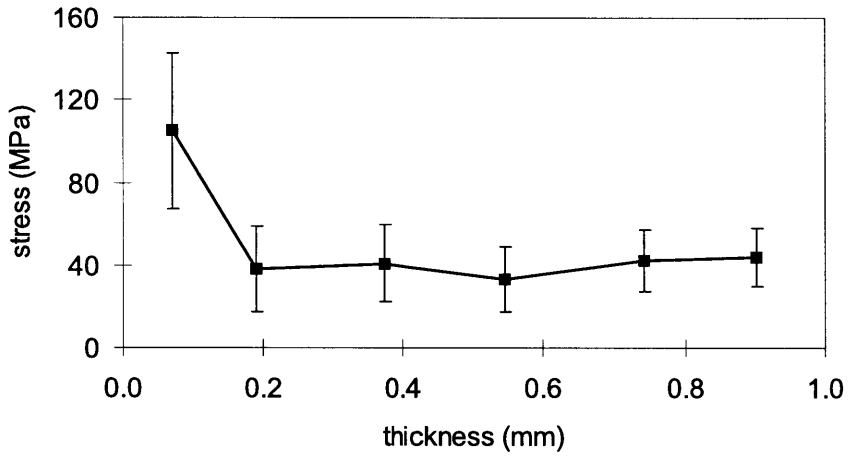

Figure 3-2: Surface stress in separate Mo coatings as a function of total coating thickness, measured by X-ray diffraction. Each point is from a different specimen.

Figure 3-3 shows corresponding data from neutron diffraction. Each data point represents the average stress in either the substrate or the entire coating of each given thickness, with each data point representing a different specimen. The average stress in the coating is slightly smaller than the surface stress, and slowly decreases with increasing thickness. This indicates a stress gradient over the coating thickness, towards tension at the surface. The gradient is a result of coating build-up by consecutive deposition of new layers; as each new layer is deposited and quenched, it

develops tensile stress, which in turn shifts the underlying layers towards compression [50,76]. The magnitude of the gradient, calculated from the X-ray and neutron data, is around 30 MPa/mm. The tensile stress in the coating is balanced by compressive stress in the substrate, whose magnitude increases as the coating thickness increases.

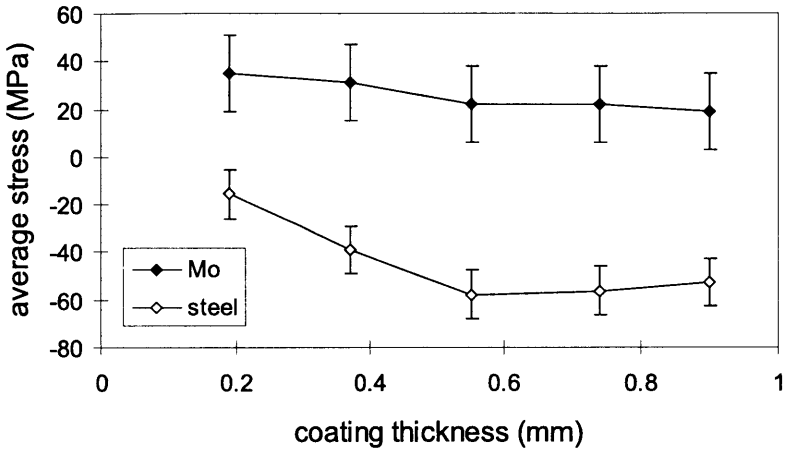

Figure 3-3: Average stresses in the individual Mo coatings as a function of total coating thickness, measured by neutron diffraction. Each point is from a different specimen. All substrates had the same thickness, 0.67 mm.

Figure 3-4 shows the average stress in each individual layer of the Mo coatings, determined by the curvature measurements, as a function of total thickness of the layer. This allows a direct comparison between the curvature and diffraction methods. It can be seen that the same trend is observed using both the curvature and diffraction techniques, but that the absolute values of the stresses are lower when calculated using the diffraction methods than with the curvature method. One possible explanation of the difference between curvature and X- ray diffraction data in the thinnest layer (not measured in the neutron diffraction experiments) comes from the nature of the two measurement techniques. The stress values from the X-ray diffraction measurements could be somewhat reduced due to surface roughness effects (due to the very low penetration of X-rays), while the curvature and neutron diffraction methods measure

the average stress in an added layer. For a thin surface layer with a high residual stress, as observed in the thinnest molybdenum layers here, this difference in the quantities measured with the two techniques could lead to pronounced differences in the absolute values of the resulting calculated stresses, as observed by comparing Figures 3-2 and 3-4.

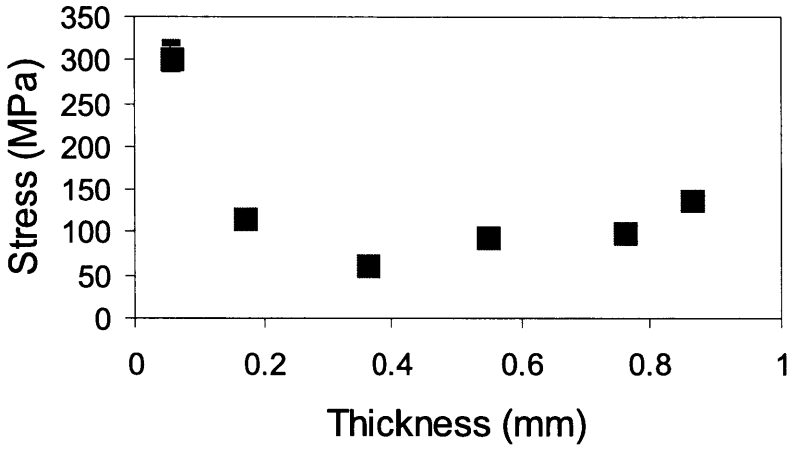

Figure 3-4: Average stress in separate Mo specimens of different thicknesses, from curvature measurements. (Error bars in the thicker coatings are within the symbols.)

Figure 3-5 shows the through-thickness stress profile as a function of position in the thickest coating of Mo on steel, as calculated from the curvature measurement technique (Chapter 2) [50]. The x values are the values of the position, in millimeters, of the center of each thin layer contained within the coating for which the residual stress was calculated. The stress values plotted are the average cumulative stress in each thin layer within the coating, located at the given position. As in the case of individual coatings, it is seen that the stress is most highly tensile in the thin layer of Mo coating that is immediately adjacent to the steel. In subsequently deposited layers, the stress decreases, possibly due to the difference between the strength of bonding of the new coating with previous Mo layers and the bonding of the new

coating with the steel substrate, and also due to possible annealing effects on the stress in previous layers caused by heat input from new layers. It can be seen from these results that, near the interface, the average stress in a thicker layer (Figure 3-4) is slightly higher than the stress at that position in the full coating (Figure 3-5), since the initial deposited layer contained a very high residual quenching stress. The difference between neutron diffraction and curvature data can also be explained at least partly by the difference in the relevant measurement areas of the substrate: the neutron diffraction measurements are localized to an area of the order of mm^2, while the curvature technique measures the stress in a thinner layer (tenths of a millimeter) over a 2-cm gage length.

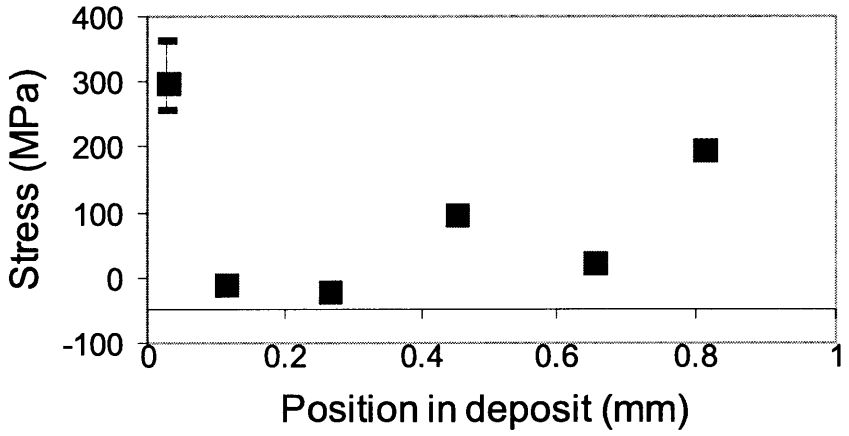

Figure 3-5: Through-thickness residual stress profile in a thick (1 mm) Mo coating on steel, obtained using the curvature technique. (Error bars in the thicker coatings are within the symbols.)

The curvature results for the full coating indicate that the value of the stress decreases sharply from 300 MPa in the first layer to approximately –20 MPa in the adjacent layers, and then climbs to higher values in subsequent layers, reaching close to 200 MPa at the surface. This may be due in part to the result of adding additional layers on top of the previous ones. The new layers experience a tensile quenching

stress and cause the intermediate layers below to shift to more compressive values of residual stress compared to the values of average stress in layers of those thicknesses without additional layers on top. However, unlike the graded coatings examined in Chapter 2, The changes in stress in the Mo layers due to the added layers on top are not all towards more compressive values, but exhibit both positive and negative values, all of which have a small absolute value.

The origin of the difference between the first and subsequent coating layers is not completely clear, but two possible explanations may be offered.

1. A difference in substrate temperature: a slightly colder substrate in the first case might lead to higher tensile quenching stress (substrate preheating and air cooling during deposition were employed to maintain a nearly constant deposition temperature of approximately 200°C; however, a short delay between preheating and spraying could possibly result in some small temperature drop).

2. There may be a difference in adhesion strength between the first and subsequent layers. The first layer is deposited on a bulk material substrate, whereas later layers arrive on top of previously deposited coating whose strength may be reduced by pores and imperfect interlamellar contact. Plasma-sprayed microstructures, as previously discussed, contain many small pores and microcracks. This is probably the limiting factor that keeps the stress at approximately constant value in the layers that are deposited on top of previously deposited layers [77].

3.3.2 Composites and FGM's

Figure 3-6 shows the stress profile in a pure Al_2O_3 coating, determined by neutron diffraction. The overall stress in the coating is compressive, with a small gradient towards tension at the surface, resulting from quenching stress. Although during the quenching stage the coating experiences a much larger temperature drop (approx-

imately 1800°C) than during the cooling stage (approximately 150°C), the thermal mismatch stress prevails. Since the thermal expansivity of Al_2O_3 is smaller than that of steel (Table 3.5), the resultant coating stress is compressive. This is in contrast to Ni-based coatings [77], whose thermal expansivity is very close to that of steel, and thus quenching is a major contributor to final residual stress. Compressive stress in the alumina coating is balanced in the substrate whose average stress is slightly tensile; the resulting bending moment leads to a stress gradient in the substrate, with tension near the interface and compression near the back surface. In order to achieve sufficient spatial resolution for the stress profiles, the gauge volume has to be quite small; then the measurements are very time-consuming. Therefore, the gradients were investigated only in this one case; in the following paragraphs, average stresses from the entire coating or substrate thicknesses are presented.

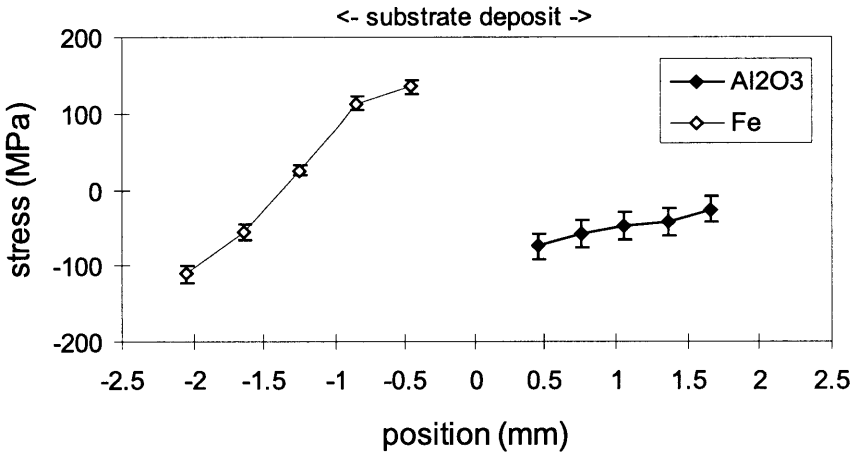

Figure 3-6: Through-thickness stress profile in the Al_2O_3 coating on steel, determined by neutron diffraction.

Figure 3-7 shows the residual stress in each phase of the single-composition Ni+ Al_2O_3 composite specimens, as well as in the substrate, as a function of coating composition in each specimen. The stresses in the pure metal and pure ceramic coating

Material	$\alpha(10^{-6\circ}C^{-1})$
Mo	5
Ni, NiCrAlY	13.3
Fe	13.5
Al_2O_3	7
YSZ	11

Table 3.5: Thermal expansion coefficients of the materials under study

are tensile and compressive, respectively, in accordance with the previous statement about thermal expansivities. In both phases, the stress increases in magnitude, while retaining the sign, as the content of this phase decreases and it is more restricted by the other phase. The average stress in the coating changes from tensile to compressive in going from pure metal to pure ceramic and is balanced by a corresponding opposite stress in the substrate.

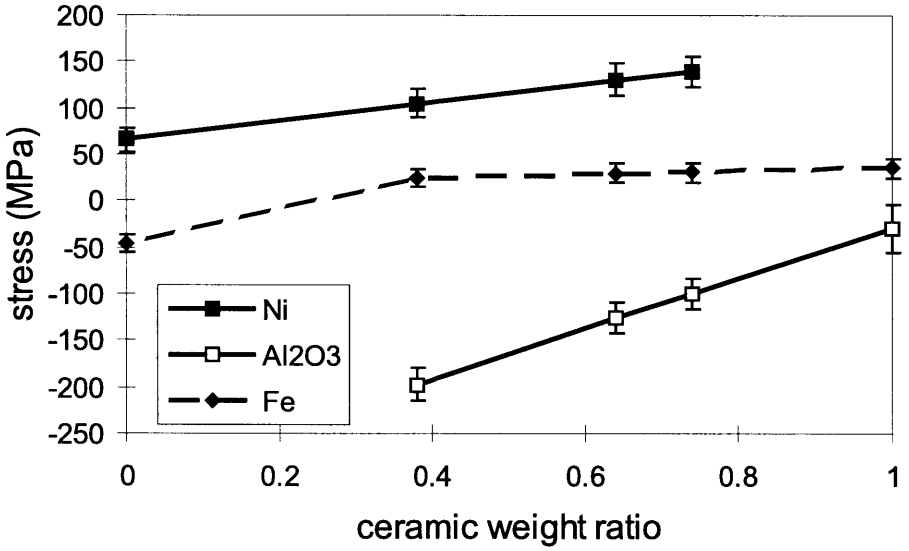

Figure 3-7: Residual stresses in Ni+ Al_2O_3 composites, by neutron diffraction

Figure 3-8 shows the average stresses in the graded single layers of Ni–Al_2O_3 com-

posites on steel substrates, obtained from the curvature data. As observed also in the neutron diffraction experiments, there is a large tensile residual stress dominated by the quenching stress in the layers with high Ni content, and low, slightly compressive stresses in the Al_2O_3-rich layers dominated by the thermal mismatch stress. Thermal cycling experiments were performed on the specimens to determine the CTE of each graded composite layer, and the results of these experiments were used to directly separate the effects of the thermal mismatch stress from the quenching stress, as discussed in Chapter 2. These results are shown in Figure 3-8.

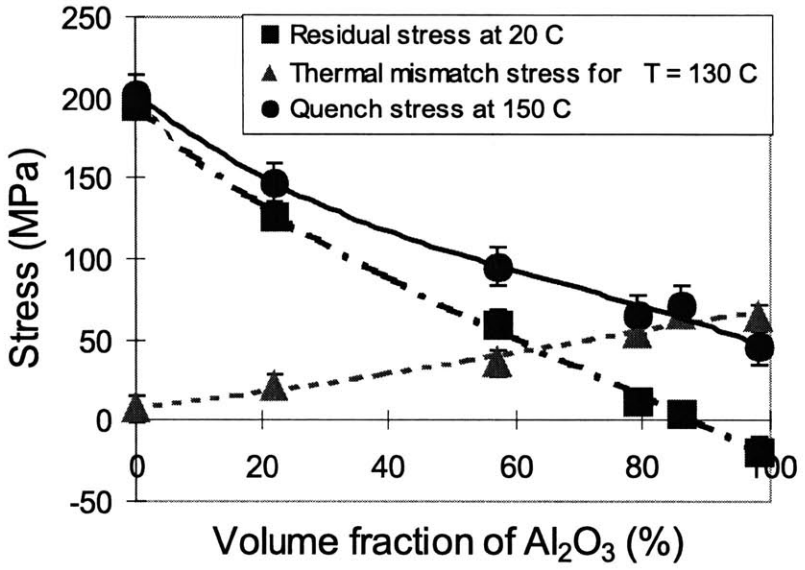

Figure 3-8: Average residual, thermal mismatch, and quenching stresses in the coating layer of separate Ni+ Al_2O_3 composite specimens as a function of average coating composition, from curvature measurements.

Figure 3-9 shows the neutron diffraction data, re-plotted as an average layer stress by taking the volume fraction of each phase into account in a linear rule of mixtures, as follows:

$$\sigma_{\text{Avg}} = f\sigma_{\text{Al}_2\text{O}_3} + (1-f)\sigma_{\text{Ni}}, \tag{3.4}$$

where f is the volume fraction of Al_2O_3, σ_{Ni} is the stress in the Ni phase, $\sigma_{Al_2O_3}$ is the stress in the Al_2O_3 phase, and σ_{Avg} is the average stress in the composite layer. When the data are plotted in this way, the same trend is observable using both the neutron diffraction and curvature techniques, with large tensile quenching stresses in the metal-rich phase on steel, and smaller, slightly compressive stresses in the ceramic-rich phase after cooling to room temperature. It should also be noted that again, the absolute value of the quenching stress in the initial layer of Ni on steel that is calculated from the curvature technique is higher than that calculated from the neutron diffraction data. In this case, however, some differences can be expected due to different specimen sizes, which are required for the different measurement techniques.

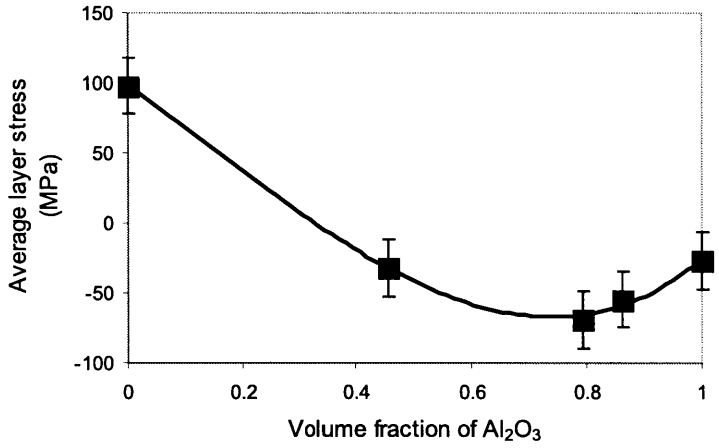

Figure 3-9: Average layer stress in the separate Ni+ Al_2O_3 composite specimens, calculated from the neutron diffraction data (for comparison with the curvature data)

The results from NiCrAlY+YSZ fixed-composition composites, shown in Figure 3-10 show trends similar to the Ni+ Al_2O_3 composites and FGMs. A difference can be observed in the case of the pure ZrO_2 ceramic, which has a slightly tensile residual stress (although close to zero within experimental error). Generally, the stresses in the ceramic phase are smaller in this case than in the nickel-alumina system; this can be attributed to lower thermal mismatch between zirconia and both steel and NiCrAlY.

The results from the curvature measurements on the graded NiCrAlY + YSZ FGMs show the same trends, as seen in Figure 3-11, with large, tensile residual stresses in the metal-rich layers that are dominated by the quenching stress, and small, slightly tensile residual stresses in the ceramic-rich layers that are dominated by the thermal mismatch stress upon cooling to room temperature from the deposition temperature. Again, thermal cycling experiments were performed to determine the CTE of each layer and to separate quantitatively the effect of the quenching stress from the effect of the thermal mismatch stress on the overall residual stress in the materials at room temperature.

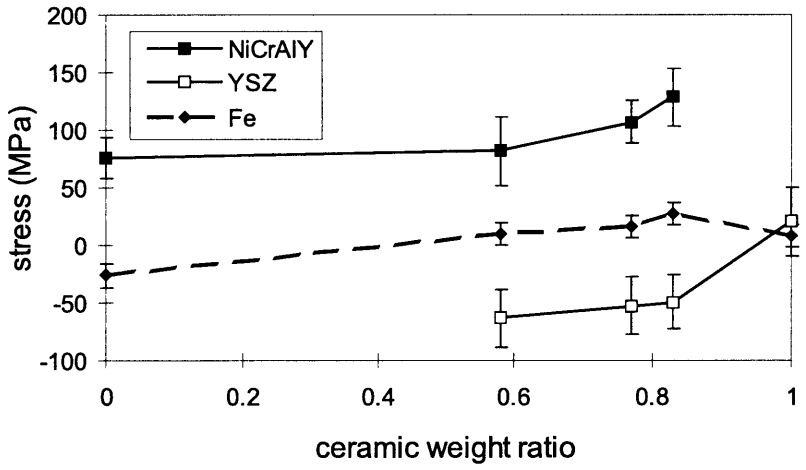

Figure 3-10: Residual stress in the individual, fixed-composition NiCrAlY+YSZ composites, by neutron diffraction

3.3.3 Sensitivity analysis

The results in this and the previous chapter have been based upon calculations in which measured values of layer thickness and curvature were used along with experimentally calculated values of curvature variation with temperature and analytically calculated values of Young's modulus with composition. Different initial values of

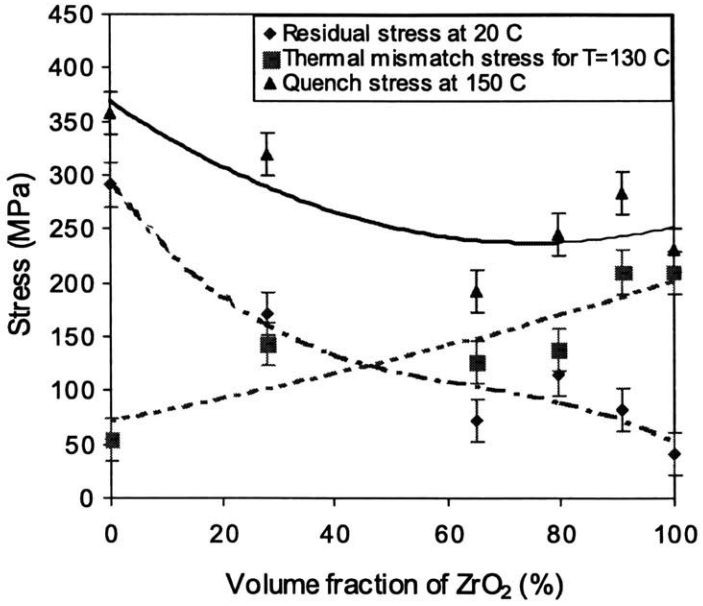

Figure 3-11: Average residual stress in the coating layers of individual, graded NiCrAlY+YSZ composites, by curvature measurements.

these material or specimen properties would result in different calculated values of the final stresses that result. To determine which of the input data are most important in their effects on the final results, a sensitivity analysis of the results was performed using the value of the quench stress in the Ni–Al_2O_3 system. The quench stress was chosen because it is a substraction of the thermal mismatch stress from the total room temperature residual stress, and thus it is influenced by all of the material and geometrical properties of the specimens.

It was found that the largest effect on the final results came from the error in the measurement of specimen thickness, both in terms of relative change in stress per change in input as well as total change in stress. It was found that for the thinnest deposited layer, a change in measured layer thickness of 0.01 mm (representing a 14.5% error) resulted in a change in quenching stress of approximately 30 MPa (a 17.4% error). In the thickest layers the effects on the error were smaller. A measurement change of 0.01 mm (4%) results in a change in the quenching stress calculation of

1.1 MPa, or 2%. This relative error is significantly smaller than for the specimens with thinner coating layers, but it is worth noting that the percentage change in the output value is on the same order of magnitude as the percentage change in the input value, making coating layer thickness a first-order influence on the calculated value of the quenching stress.

The factor with the next largest effect on the values of the quenching stress is the Young's modulus. The uncertainty in the experimental and analytical calculations of the Young's modulus ranged from one-sixth to approximately one-half of the bulk modulus. This range of values for the Young's modulus also leads to a range in values for the final quenching stress. Specifically, a relative change in the Young's modulus of 50% resulted in a change in the final quenching stress of 5% (11 MPa) in the thinnest layer, and of 33% (24 MPa) in the thickest layer. Thus it can be seen that the effect of the Young's modulus variation on the variation in quenching stress is a second order effect, with the relative error in the final output values of quenching stress being approximately one order of magnitude lower than the relative error in the input values of Young's modulus for the coating layers.

The smallest influence on the final values of quenching stress from the input factors is the influence due to the error in measurement of curvature variation with temperature. It is these measurements from which the coefficient of thermal expansion of each layer is calculated, and it is also these measurements which are made with the highest precision by the laser-based curvature measurement apparatus. A typical curvature measurement error of 0.6% results in a quenching stress error of 0.02% (0.047 MPa) in the thinnest layer, while the same resolution of curvature measurement, resulting in a relative error of 0.03% in the thickest layer, results in a relative change in the quenching stress of 0.04%. Thus the relative error introduced into the final calculation of the quenching stress due to an error in curvature change value is from 1 to 0 orders of magnitude different from the percentage change in the curvature values themselves.

Thus, the sensitivity of the results to the change in various input factors is highest for the thickness measurements, next highest for the curvature measurements which lead to values of the CTE, and lowest for the values of the Young's modulus. However, the actual influence of these factors on the final measurements of quenching stress depend not only on the sensitivity of the quenching stress to the various errors but also on the magnitude of each of those errors. Thus, combining the sensitivity of the results with the expected error in the input values, we find that the results are most affected by errors in the thickness measurements, followed by errors in the Young's modulus calculations or values, followed by errors in the curvature variation with temperature that is used to calculate the Young's modulus of each coating layer as a function of composition.

3.4 Conclusions

Three different methods were used to determine the residual stresses in three different layered and graded coating systems, Ni + Al_2O_3, NiCrAlY+ ZrO_2, and Mo on steel substrates. The use of a combination of three different techniques allowed a more complete determination of the coating material system properties and stresses, which would not have been possible with the use of only one technique alone. The methods used are complementary, and each can supply unique information for different material systems and experimental situations. For example, the separation of thermal mismatch stress and quenching stress contributions to total residual stress, as well as the thermal expansion coefficients of composite layers, can be made quite conveniently with the curvature technique, and this has been done for the Ni–Al_2O_3 and NiCrAlY-YSZ systems studied here. The neutron diffraction technique, on the other hand, can distinguish the stresses in the different phases of a coating, as presented here for the Ni and Al_2O_3 coatings on steel. Both allow determination of average stress in a thick layer and through-thickness stress profiles in thick coatings, as pre-

sented here for homogeneous molybdenum coatings on steel. However, the curvature method allowed a finer resolution of stress measurements to be made in the coatings, allowing a more localized determination of stress to be made, particularly in the thin deposit layers of plasma-sprayed metal in direct contact with the substrate, which tended to be thin layers with high values of tensile stresses. X-ray diffraction allows determination of the stress in a very thin surface layer of the material (20–30 μm), for cases where only the localized surface stress is of practical interest. Thus, the information from each of the techniques can be combined to obtain a more complete picture of the residual stresses in coatings produced by a variety of techniques, such as plasma spraying. This information, in turn, can be used to control the stresses by modifying the processing parameters, such as the deposition temperature [77], spraying distance or atmosphere during processing. In addition, the composition profiles of the graded coatings can be adjusted along with the processing parameters in order to reduce the magnitude of residual stresses or to obtain an optimal pattern of compressive and tensile stresses in coatings for a given design application. These and additional implications for coating design decisions and selection of property and stress determination techniques for the study of coatings will be discussed in more detail in Chapter 5.

Chapter 4

Local property determinations in surface coatings

4.1 Introduction

In order to perform the residual stress measurements described in the previous two chapters, it was necessary to know or experimentally determine the thermo-elastic material properties (Young's modulus, E, and coefficient of thermal expansion, α) as a function of composition for the temperature range being studied.

The curvature measurement technique combined with the successive build-up of layers, described in Chapter 2, provides an average stress in each discrete layer, and also measures the average thermo-mechanical material properties of each layer. The coefficient of thermal expansion calculated using the procedure described in Chapter 2 is an average coefficient of thermal expansion for each layer of graded (or fixed) composition for which the thermal cycling experiments are performed. In addition, the determination of Young's modulus using the analysis in Chapter 2 combined with four-point bending experiments also provides the average value of the Young's modulus within the entire layer that is measured using the technique. However, unlike the diffraction experiments, the Young's modulus that is significant in the

case of the curvature measurements, and that is measured using the 4-point bending technique, is the in-plane Young's modulus, in the plane of the deposited coatings. Because of the anisotropic nature of coatings that are deposited by plasma spray deposition, the in-plane properties can be substantially different from the volume-averaged coating properties, as discussed in Chapter 2 in relation to the coefficients of thermal expansion of the coatings. It is the in-plane elastic properties of the material that contribute to the values of the in-plane stresses, and those in-plane stresses are the only non-zero stresses in the equi-biaxial stress states resulting from the deposition of coating layers on a substrate that is much wider in the x and $y-$dimensions than the thickness in the $z-$direction of the coatings (away from the edges of the specimen).

In both the neutron diffraction and x-ray diffraction experiments, in contrast, the bulk material properties were used, since the diffraction measurements measure a three-dimensional volume-averaged strain within a very localized region of material. Since only the change in lattice spacing is measured, these two diffraction techniques inherently determine the stresses within single-crystal grains of the material, and these single-crystal stresses are locally averaged over the spot size of the x-ray or neutron beam, providing a localized measurement of three-dimensional stresses, using the bulk properties of the materials.

However, as discussed previously, coatings deposited by plasma spray deposition will not have the same properties as the bulk materials, even in the plane of the coatings, although the deviation from bulk properties may be expected to be higher in the direction perpendicular to the plane than in the directions within the plane. For cases where there is interest in determining the average three-dimensional properties of the coatings, rather than using the bulk properties for stress determinations such as by x-ray or neutron diffraction, another experimental technique can be employed to accurately determine the three-dimensional properties of coating materials, using instrumented quantitative spherical or sharp indentation experiments [14,55,78-81].

Indentation experiments can be used to determine the localized elastic and plastic properties of the coatings, within a range of distance around the indentation location of approximately 5–7 times the indentation dimensions, such as contact radius. These experimental property determinations can then be used in conjunction with three-dimensional stress measurement techniques such as diffraction measurements, in order to find a more accurate determination of the stresses than can be calculated by simply using the bulk material properties.

In addition, theory also exists [14] to allow instrumented sharp indentation to be used to obtain a measure of the equi-biaxial residual stress state existing near the surface in an elasto-plastic material. This stress value will be an average value of the equi-biaxial stresses existing below the surface, over a depth of approximately 5–7 times the depth of the indentation used to detect and calculate the material properties and stress state. However, there is currently no theory that allows the residual stress state to be similarly calculated for inhomogeneous materials containing a non-zero content of ceramic (or other fully-elastic material) in or near the surface layer, without inducing controlled cracking (which is difficult in plasma-sprayed coatings). However, such experiments can be performed on metallic materials to probe the near-surface equi-biaxial stresses and volume-averaged properties.

The localized properties of materials can be determined on a variety of size scales using a variety of indenter sizes and loads, to produce a variety of indentation depths and indentation contact radii. These size scales range from the nanoscopic to the microscopic to the macroscopic. When plasma-sprayed materials are studied, this variation can correspond to examining the localized properties of the microstructure on the size scale of the individual splats (micro-indentation), or on a wider size scale over which the properties of many individual splats are averaged (macro-indentation). To probe the properties of a single-splat of a plasma-sprayed material, care must be taken to ensure that the indentation is made entirely within a splat, and not in the regions of inter-splat porosity or microcracks.

In this chapter, localized microscopic property determinations were made for single splats of plasma sprayed molybdenum coatings on steel, using instrumented sharp indentation. The results are discussed in the context of the more distributed property measurements presented earlier in Chapter 2.

4.2 Indentation theory

Either spherical or sharp indentation can be used to determine the elastic properties of materials (see, for example, [78-80]), but through the use of sharp indentation, the residual stress state in elasto-plastic materials can also be determined if that stress state is uniform over a sufficient depth into the material. A detailed analysis of the use of indentation data for the determination of residual stresses and material properties can be found in [14]. Some key features of the analytical framework are presented here. When the variation of force with depth is measured during indentation with a sharp indenter and plotted, a P–h curve such as the one shown in Figure 4-1 is produced. During the loading portion of the curve, Kick's law is followed:

$$P = Ch^2, \tag{4.1}$$

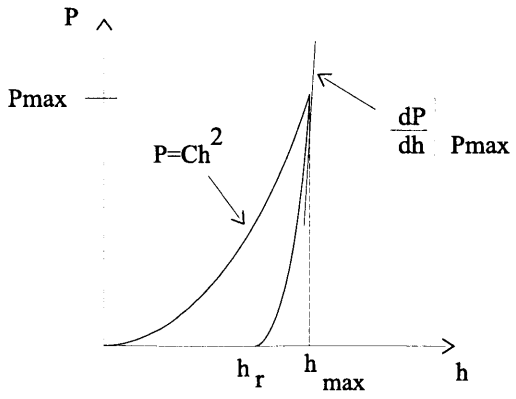

Figure 4-1: Typical variation of load versus depth during loading and unloading during indentation with a sharp indenter [after 14]

where C is a constant that depends on the elastoplastic material properties, the residual stress, and the geometry of the indenter. Upon unloading, the initial elastic portion of the unloading curve has a slope that is proportional to the elastic modulus of the material. If the elastic properties of the indenter material are known, then the elastic modulus of the indented material can be calculated from a measure of this initial unloading curve slope, as follows:

$$E = \frac{(1-\nu^2)E^* E_{in}}{E_{in} - (1-\nu_{in}^2)E^*}, \tag{4.2}$$

and

$$E^* = \frac{1}{C^*\sqrt{A_{max}}}\frac{dP}{dh}. \tag{4.3}$$

Here, E_{in} is the Young's modulus of the indenter, $\frac{dP}{dh}$ is the initial unloading slope of the P-h curve, C^* is a constant dependent on the indenter geometry ($C^* = 1.142$ for the Vicker's indenter), and $A_{\max}$ is the maximum contact area of the indentation. Thus, if the contact area and P–h curve can be accurately measured, the elastic modulus of the material can be determined. If a resdiual stress-free P–h curve for the same material can also be obtained, then the properties of the material can be determined without an experimental measurement of the maximum contact area, which is often a difficult quantity to measure accurately, if the material deforms very little plastically upon indentation.

In addition to calculating the elastic properties of the material, the plastic residual strain, yield stress, and strain hardening exponent can be determined through use of P–h curves together with experimentally measured indentation areas (see [14] for details). In addition, the magnitude of the equi-biaxial residual stresses in the material can be determined quantitatively, and by the comparison of the P-h curve of the residually-stressed material to that of a stress-free material, the sign of the residual stresses can also be determined. If the material has a compressive residual

stress, then the penetration of the indenter into the depth of the material will be more difficult, and the compliance of the indentation behavior of the material will decrease. On the other hand, if the material is in a state of tensile residual stress, the indentation will be easier to perform, and the effective compliance of the indentation will increase. These trends are shown schematically in Figure 4-2.

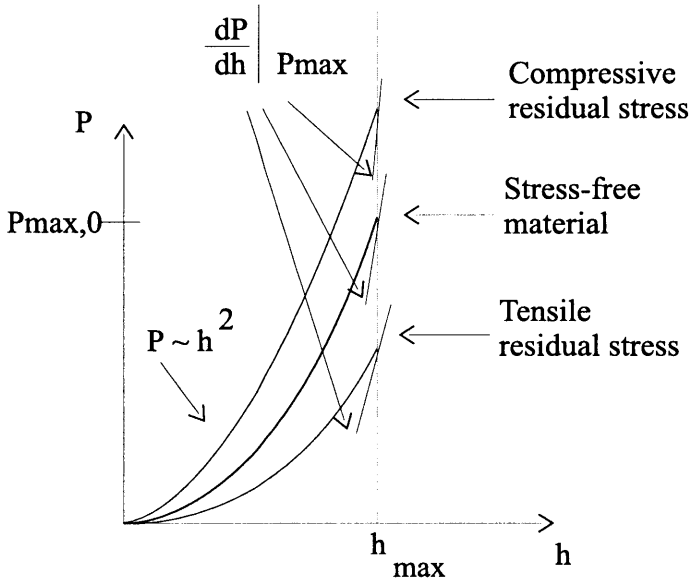

Figure 4-2: Change in compliance of the load vs. depth for materials in tensile and compressive residual stress states [after 14]

4.3 Experimental procedure

4.3.1 Specimen preparation

Because molybdenum coatings are useful as wear-resistant coatings in the automotive industry and they exhibit elasto-plastic material behavior that can be analyzed using the available indentation theory, Mo was chosen as a coating material system to examine by sharp indentation. Six specimens of thick Mo coatings deposited on steel substrates were prepared by atmospheric plasma spray processing, using a PlasmaTechnik PT-F4 torch (Sulzer-Metco Inc., Westbury, NY) (see Figure 2-6). The

substrates were held at different temperatures during the deposition process, ranging from 150°C to 330°C.

4.3.2 Indentation experiments

Each of the specimens was indented 10 to 15 times using an Instron Wilson MicroRockwell testing machine (Instron Corporation, Canton, MA) with a diamond Vicker's pyramid indenter (square pyramid). The indentations were performed to a load of 10 Newtons in order to obtain indentation sizes which were smaller than but on the same order of size scale as the relevant microstructural features of the specimens, which in this case are the individual splats formed by the plasma spray deposition process. Before each group of tests was carried out, 10 indentation tests were performed on a sample material to linearize the voltage signal in the load cell. Ten indentation tests were then performed on a series of known materials, including aluminum and several steels and brasses, in order to calibrate the indentation machine compliance. The value of machine compliance obtained from the calibrations was then used to evaluate the experimental test results obtained from the test specimens with unknown properties. A schematic diagram of the indentation apparatus is shown in Figure 4-3.

During each indentation test, the load and depth of penetration were continuously recorded during both loading and unloading. The indentations were made at distances of at least 0.6 mm apart, a distance which is substantially larger than three times the indentation diameters. The indentations were then examined with an optical microscope.

4.4 Results and discussion

Since similar results were obtained for each of the six specimens studied, typical results are presented here only for one of the specimens, a Mo coating deposited 330°C. The

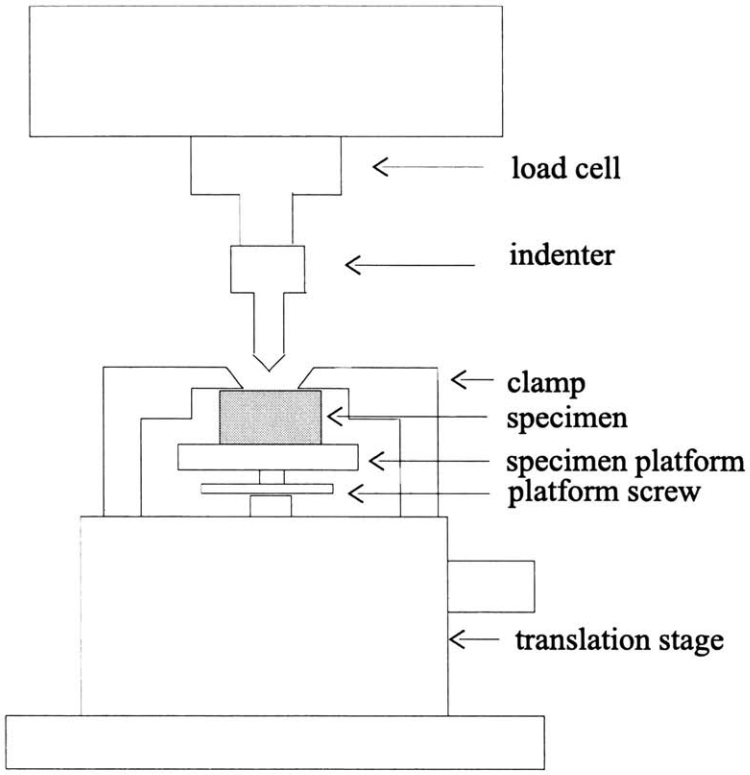

Figure 4-3: Schematic diagram of indentation apparatus used

initial load vs. depth curves during loading and unloading for 10 indentations across the surface of the specimen were made, and used to calculate the Young's modulus and Vicker's hardness of the specimens. After testing, the indentations were studied with an optical microscope. Due to the large variation in surface roughness on the scale of the indentations performed, there was a wide range of indentation sizes, and most of the indentations were irregularly shaped, leading to a fairly large scatter in the measurements of the contact areas of the indentations. This is a direct result of the nature of the microstructures of plasma sprayed materials, since these materials have many microcracks and pores, and are highly anisotropic in nature. The average dimension of the indentation diagonals over all of the specimens measured was 60.8 $\pm$ 15.8 μm, while the typical splat diameters were approximately 150 $\pm$ 10 μm and the typical splat thickness were approximately 10.7 $\pm$ 3 μm.

Depending on the location where the indentation is made on the surface of the

specimen, substantially different properties can be observed, as a function of whether the indentation is centered on a splat of the material or on a crack or a pore. An indentation that is fully contained within a splat of the material detects localized single-splat properties, while an indentation centered on a crack or a pore will result in an average material property for the sampled material that has a lower stiffness and hardness. Study of the P-h curves suggested that many of the indentations resulted in cracking or other jumps in the depth of penetration at a constant load. This is to be expected due to the nature of the microstructures of plasma sprayed materials, as was seen in the previous chapters. However, if the properties of a single-splat are desired rather than an average of the behavior of the full coating including the defects such as cracks and porosity, then only indentation curves that penetrate the interior of such a splat should be considered. In other words, only curves whose behavior does not suggest the presence of specimen cracking are relevant in the study of the localized single-splat properties of the specimens.

Thus, only the graphs exhibiting continuous load vs. depth curves with no sudden discontinuities were used for the analysis of the local properties, while all of the curves were used to determine the "average" coating properties. Three such single-splat load-depth plots for the specimen are shown in Figure 4-4. There is some variation between the curves, but it is substantially less than the amount of variation that can be observed when probing the entire plasma-sprayed surface.

No stress-free reference was available for the materials studied, so it was not possible to calculate the value of the residual stress in the specimens by comparison to a known P–h curve, as discussed in relation to Figure 4-2. In order to calculate the stress without such a stress-free reference curve, accurate measurements of the indentation area are needed, and for this, the indentation would have to be performed on a size scale that would be substantially larger than the characteristic size scales of the plasma-sprayed microstructural features, so that the value of the measured area would not be significantly affected by the local variations in topography of the

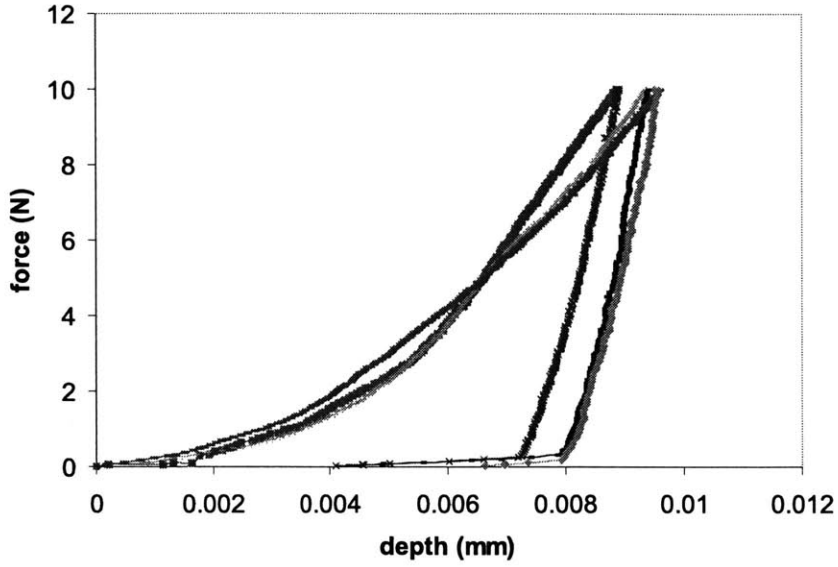

Figure 4-4: Continuous (single-splat) load vs. depth curves for plasma-sprayed Mo

surface. To obtain the values of the stress on a more macroscopic, volume-averaged scale, a much larger indenter would need to be used. This could be one way to obtain a more easily measurable indentation contact area, which could in turn allow a more quantitative assessment of the residual stress state in the surface of the coatings to be deduced from the indentation experiments alone.

The volume-averaged elastic modulus and Vicker's hardness of the material, on the other hand, were determined for the coating from the P–h curves obtained in the indentation experiments. These calculations are of an average value of the relevant property over the volume of influence of the indentation, as if the material were homogeneous and isotropic over the sampled volume. In reality, the material is both anisotropic and inhomogeneous, so the property values calculated from the load–depth response are the averaged values over the entire volume of material that is affected by a given indentation. These values were calculated for both the local, single-splat indentations, and for the average of all of the indentations performed over the large

	E (GPa)
localized	180 ± 9
large volume	135 ± 46
bulk	335 ± 10

Table 4.1: Young's modulus of the Mo coatings as determined from indentation experiments, and a comparison with bulk values

volume, including those that were performed over cracked or porous regions of the specimen. The results are shown in Table 4.1. It can be seen that both the hardness and the Young's modulus of the single splats of the coating are substantially higher than the averaged values obtained from a combination of all indentation results from the surface of a specimen. In addition, the table shows that, as expected from the inhomogeneous character of the coating surface, the scatter in the values is much higher for the large-volume results than for the single-splat results.

4.5 Conclusions

The local single-splat elastic modulus and Vicker's hardness of plasma-sprayed Mo coatings on steel substrates were determined through the use of quantitative sharp indentation experiments using a Vicker's diamond pyramid indenter. In general, micro-indentation experiments carried out with suitable loads and penetration depths can be used to determine local volume-averaged properties within a plasma-sprayed coating, allowing a single-splat property determination to be performed. In addition, by increasing the size of the indenter and/or the indenter load, the volume-averaged properties of a larger region can determined as well. In addition, the trends in the equi-biaxial residual stress state of an elasto-plastic material can in theory be observed qualitatively, and through a comparison with a stress-free reference or precise experimental measurements of the indentation contact area, a quantitative determination of the absolute value of the residual stress could also be obtained, although

these experiments were not done here. Together with the other techniques studied in Chapters 2 and 3, instrumented indentation provides one more tool that can be used to determine a variety of different properties of interest in the study of layered and graded coating materials which can not be readily studied through more traditional methods of studying bulk materials.

Chapter 5

Concluding remarks

5.1 Implications of the work

5.1.1 Selection of appropriate experimental techniques

An experimental method has been developed as part of this work to determine the residual stresses at room temperature, the intrinsic stresses at the processing temperature resulting from any deposition process, and the thermal mismatch stress resulting from a cooling from the deposition temperature, as well as the coefficient of thermal expansion and Young's modulus of layered or graded coating materials, as a function of position in the deposit thickness, and as a function of temperature for a given deposit composition or location. This method has been used, along with other complementary techniques, to determine the residual stresses and thermo-mechanical properties of a variety of layered and graded coating materials. Each of the techniques has different strengths and weaknesses, and different conditions in which they are most convenient, useful, or valid. Some of these conditions are summarized below in Table 5.1.

It can be seen that the four techniques used to study the coating materials are complementary, and a well-chosen combination of techniques allows the performance of a

more complete materials evaluation than could be obtained from just one technique alone. Furthermore, the complementary nature of the techniques suggests different conditions in which each technique could be the most useful for a given property and stress determination task. A partial list of such conditions follows for each technique, to aid in the selection of the best tool for each material system to be studied:

- X-ray diffraction: When a quick determination of only the surface residual stresses in a very thin surface layer of a material is of interest, this technique provides a quick way to determine the stress in the material, with a fairly simple experimental set-up. Best for either homogeneous materials, or when the phase-specific stresses in a composite are of interest.

- Neutron diffraction: If thick specimens of very irregular geometries are to be studied, neutron diffraction may be the only way to determine the stresses accurately, but with a low (mm-scale) resolution. Also useful when a non-destructive stress evaluation of an already-used material is required. If large-scale phase-specific stresses are needed, this is the easiest technique to obtain that information.

- Curvature: When information about material properties is unknown and flat specimens are to be studied, this is a simple technique for determining the stresses and material properties, with both through-thickness capabilities and also fine-scale resolution. This is the only of the four techniques described here that specifically allows in-plane properties to be determined, rather than three-dimensional properties. Easiest technique for separating the different components of stress.

- Indentation: When localized properties on any size scale are of interest for flat specimens, indentation is a fast, simple technique to determine the properties quickly, with a wide range of resolutions.

Strip curvature	Neutron diffraction	X-ray diffraction	Indentation
average values from a layer	phase distinctive	phase distinctive	localized average
requires thin, flat substrates	requires thicker coatings	no requirements on thickness	requires flat surfaces
can resolve finely graded coatings	virtually no limit on size or shape, but resolution limited to mm scale	analyzes only thin surface layer (tens of μm)	high resolution, many size scales
can separate quenching and thermal stresses by relatively simple method	can deconvolute quenching and thermal stresses in some cases, if material properties known	same as neutron diffraction	same as neutron diffraction
can determine stress profiles when specimens of different thickness are prepared (with assumptions)	can determine stress profiles in thick coatings non-intrusively	cannot be applied to depth without material removal	samples surfaces stresses only, but on an adjustable size scale
relatively simple experimental procedure	complex, costly, and time-consuming experimental procedure	relatively simple measurement procedure	relatively simple measurement procedure
captures in-plane properties – anisotropic	three-dimensional properties	three-dimensional properties	three-dimensional properties

Table 5.1: Comparison of four techniques for residual stress determination in layered and graded coatings

5.1.2 Coating properties and design

Through a combination of experimental techniques, the trends in processing-induced residual stresses and thermo-mechanical properties of a range of metallic, ceramic, and composite layered and graded coatings were examined. Some key trends were observed across all of the plasma-sprayed coating material systems studied, and these are summarized here:

- Materials deposited on similar materials (i.e. metal-rich coatings on metallic substrates or other metal-rich coatings or ceramic-rich coatings on other ceramic-rich coatings) retain the largest residual stresses.

- Mixtures of metal and ceramic in combination with either pure metals or pure ceramics experience the lowest stresses, while still remaining bonded to the substrates or to the previously-deposited layers.

- Ceramic-rich layers at the surface of a thick coating have the highest tensile stresses, and are thus potential sites for the initiation of cracking in graded coatings.

- Materials below the surface of a coating experience a small shift towards more compressive stresses as new layers of different compositions are deposited on top of them.

- In agreement with previous literature results, the Young's modulus of plasma-sprayed coatings was found to be lower than the corresponding bulk property values. In constrast, the values of coefficient of thermal expansion were found to be comparable to the values for composites of bulk materials.

These trends that were observed through the experiments in this work suggest some possible approaches toward the improvement of coating design and coating properties. Some possible strategies include:

- Utilizing graded coatings beginning with a mixture of metal and ceramic deposited on metal to reduce the high tensile interfacial stresses that occur between pure metallic coating layers and metallic substrates, to decrease the risk of debonding at the interface between coating and substrate.

- Varying the composition profile from linear to parabolic or other non-linear profiles, to re-distribute the locations of the stresses in a coating into a more favorable or less deleterious distribution.

- Adding a reverse-graded layer on top of a full coating to decrease the tensile stress in the pure ceramic component of the coating (in cases where the application allows a mixture of metal and ceramic to exist on the surface, such as low-temperature applications).

- Altering the deposition temperature during the production of the coating to change the relative influence of thermal mismatch stress during cooling and the tensile quenching stress due to the initial deposition. By increasing the temperature of the substrate, for example, the relative importance of the thermal mismatch stress upon cooling is increased and the relative importance of the quenching stress is decreased. Since the quenching stresses are always tensile in the plasma spray deposition process and the thermal mismatch stresses are compressive in ceramic layers on metallic substrates, this is a way to decrease the stress in the ceramic surface layers and make it more compressive, thus reducing the probability of brittle failure.

- Altering other processing parameters in order to change the effect of the intrinsic quenching stress. Examples include the atmosphere in the deposition chamber, the speed of the plasma gas jets, or the distance between the spraying nozzle and the substrate. Each of these factors could influence the final residual stress produced as a result of processing. Stress measurements like the ones performed in this work can be done for each set of processing parameters to determine

their effect on the final stress state, and the parameters can then be adjusted accordingly to obtain the desired influence on the residual stress in the coatings for a given design application.

5.2 Summary

Layered and graded coating materials, with carefully-introduced variations in properties and compositions, are important in a wide variety of practical applications, in both thin and thick films. The extensive use of coating systems for a variety of industrial needs results in the need for a thorough understanding of how such coatings will behave in various service conditions. Such an understanding depends on a good knowledge of the coating properties, which can differ substantially from bulk material properties, and of the residual stress states which remain in the coatings as a result of the processing. Residual stresses in the coatings can significantly alter the performance and lifetime of coatings, and so a knowledge of the residual stress state is important in designing a coating to withstand the additional service loading conditions.

Prior to this work, thin film coatings with applications in the micro-electronics industry had been extensively studied and well- understood. Thick and homogeneous coatings with applications as thermal barrier coatings had also been widely studied, with additional experimental difficulties presented by the need to independently determine the elastic and thermal properties of the coatings. However, thick, non-homogeneous coatings, such as functionally graded material (FGM) coatings that have recently become more widespread in various industrial applications, were less readily understood, or studied experimentally, and no standard techniques existed for their property and stress determination. Thus, the goal of this work was to improve the understanding of the residual stress states and material properties of thick layered and graded coatings, including the introduction of a new experimental technique in

order to make the property and stress determinations of such coatings more readily performable.

A summary of the key results from each chapter are presented here:

- Chapter 1 discusses some applications of coating materials examined in this study and provides a motivation for the study of their properties and stresses.

- Chapter 2 introduced a new methodology for determining residual stresses in layered or graded materials by use of successive build-up of material layers coupled with curvature measurements. The new method allows determination of processing-induced stresses through the thickness of the coating, the in-plane Young's modulus, E, as a function of the coating thickness, the coefficient of thermal expansion, α, as a function of the coating thickness, the variation of E and α as a function of temperature at any thickness location within the coating, and the separation of thermal mismatch and quenching stresses. The new method was used to determine the stresses and properties of a graded Ni-Al_2O_3 coating system.

- In chapter 3, a range of coating-substrate systems were studied and their stresses determined, including Ni-Al_2O_3 , NiCrAlY-ZrO_2, and Mo coatings on steel substrates. The new technique presented here and two more-traditional techniques, x-ray diffraction and neutron diffraction, were used to study the coatings, in order to obtain a more complete understanding of the material behavior and properties. The implications of the results were discussed in terms of the conditions for which each technique is most useful and valid for the study of a particular material or material property.

- Chapter 4 presented preliminary results for local property determinations of Mo coating materials on steel, using another complementary technique, sharp indentation. Experimental results and a general discussion of the technique were provided.

- This chapter presents a summary of the conclusions from this work, along with some of the implications and suggestions for future research directions based on the results obtained here.

With reference to the original goals of this work, the following objectives have been achieved through the studies presented here:

1. The residual stresses and thermo-mechanical properties in a variety of FGM and layered materials have been determined. This is the first time that the stresses and properties have been determined for functionally graded materials.

2. The separate contributions to the total residual stress state of coatings from the the different stress components have been quantitatively determined.

3. New methodologies have been developed for the evaluation of stresses and properties in thick and/or graded coating materials that are relatively simple to implement.

4. The new methodologies have been experimentally verified by using them to evaluate the residual stresses and properties of coating materials.

5. The results and conditions of suitability for the new and previously-used materials evaluation techniques have been compared.

6. The data obtained through the residual stress and property determinations have been used to provide a better understanding of the behavior of coating materials and practical methods of optimizing their properties have been suggested.

5.3 Suggestions for future work

"Prediction is hard, especially about the future." -Yogi Berra

Many possibilities exist for future directions in which to pursue the results of the work presented here. Additional experimental studies of different material systems are useful for the understanding of coating systems used for additional applications. In addition, it would be advisable to examine new coating composition profiles of the material systems already studied here, and to evaluate their in-service performance, based on the suggestions presented for improving the coating properties. In addition, studies similar to the ones performed in this work could be performed on materials that are produced with different processing techniques in order to gain a better understanding of the sources of residual stress that are introduced by each individual processing method. All of the methods used in this work are equally applicable to coatings produced by any deposition method, and so such studies would allow additional insights to be gained into the sources of stress that result from other methods of producing coating materials.

The local property studies performed on the coatings could be complemented by additional indentation experiments on different size scales and on an additional range of materials. This would also allow a direct comparison of the volume-averaged properties obtained in three dimensions by a macro-scale indentation, and in the plane of the coatings by, for example, four-point bending tests. Such work would provide additional insight into the extent of anisotropy of coating properties in- and out- of the plane of the coatings, which in turn could lead to a better understanding and prediction of the behavior of coatings before they enter service. Finally, additional three-dimensional property determinations could be performed in ceramic and composite coating materials, for example, by spherical indentation. Such experiments would complement well the studies of elasto-plastic coating materials studied here, and any of the above suggestions would provide a good complementary study to the examination of layered and graded coating materials described in this work.

"If we don't change our direction, we're liable to end up where we're headed." -Dr. John H. Gibbons, science advisor to U.S. President, 1992-1998

Bibliography

1. B .H. Rabin and I. Shiota, Editors, Special Issue on Functionally Gradient Materials, *MRS Bulletin* 20, 1995.

2. K. Barthel and S. Rambert, 5th International Symposium on Functionally Graded Materials, Dresden, Germany, October 1998.

3. Ch. Gerk and M. Willert-Porada, 5th International Symposium on Functionally Graded Materials, Dresden, Germany, October 1998.

4. Functionally Graded Materials, Ed. J. B. Holt, M. Koizumi, T. Hirai, Z. Manir, Ceramic Transactions, Vol. 34, American Ceramic Society, Westerville, Ohio, 1993.

5. S. Suresh and A. Mortensen, Fundamentals of Functionally Graded Materials, IOM Communications, Ltd., London, 1998.

6. A. E. Giannakopoulos, S. Suresh, M. Finot, and M. Olsson, *Acta Metall. Mater.*, 43:1335, 1995.

7. M. Finot, S. Suresh, C. Bull, and S. Sampath, *Mat. Sci. Eng. A*, 59, 1996.

8. E. Weissenbek, H. E. Pettermann, and S. Suresh, *Acta Mater.*, 45(8):3401 1997.

9. R. L. Williamson, J. K. Wright, and K. J. Maggs, *Mat. Sci. Eng.*, 187:87, 1994.

10. J. T. Drake, R. L. Williamson, and B. H. Rabin, *J. Appl. Phys.* 74:1321, 1993.

11. E. A. Fitzgerald, Y.-H. Xie, D. Monroe, P. J. Silverman, J.-M. Kuo, A. R. Kortar, F. A. Thiel, B. E. Weir and L. C. Feldman, *J. Vac. Sci. and Technol.*, B10:1807, 1992.

12. Soc. for Experimental Mechanics, *Handbook of Measurement of Residual Stresses*, Ed. Jian Lu, Fairmount Press, Inc., Lilburn, GA, 1996.

13. T. W. Clyne and S. C. Gill, *J. Therm. Spray Technol.*, 5(4):401, 1996.

14. S. Suresh and A. E. Giannakopoulos, Acta. Mater., 46(16), 5755, 1998.

15. G. G. Stoney, *Proc. R. Soc. London Ser. A*, 82:172, 1909.

16. M. Gudge, D. S. Rickerby, R. Kingswell, and K. T. Scott, *Proc. 3rd Int'l Therm. Spray Conf.*, pp. 331-337, Long Beach, CA, 1990.

17. D. J. Greving, E. F. Rybicki, and J. R. Shadley, *Proc. 7th Nat'l. Spray Conf.*, pp. 647-653, Boston, MA, 1994.

18. P. Bialucki, W. Kaczmar, and J. Gladysz, *Advances in Thermal Spraying; Proc. 11th Int'l Therm. Spray Conf.*, p. 837, Welding Institute of Canada, Pergamon press, 1986.

19. M. K. Hobbs and H. Reiter, *Thermal Spray: Advances in Coatings Technology*, pp. 285-290, ASM, 1988.

20. S. C. Gill and T. W. Clyne, *Metall. Trans. B*, 21:377, 1991.

21. S. C. Gill and T. W. Clyne, *Proc. 7th Nat'l Spray Conf.*, pp. 581-586, Boston, MA, 1994.

22. S. C. Gill and T. W. Clyne, *Thin Solid Films*, 250:172, 1994.

23. S. Kuroda, Colloquium, SUNY, Stonybrook, NY, 1996.

24. A. L. Shull, H. G. Zolla, and F. Spaepen, *Proc. MRS Fall'94 Symp. on Thin Films: Stresses and Mechanical Properties V*, Boston, MA 1994.

25. T. W. Clyne and Y.C. Tsui, *3rd Int'l. Symp. on Structural and Functional Gradient Materials*, Lausanne, Switzerland, 1994.

26. S. J. Howard and T. W. Clyne, *Proc. 7th Nat'l Spray Conf.*, Boston, MA, 1994.

27. A. C. Leger, A. Grimaud, P. Fauchais, and C. Catteau, *National Thermal Spray Conf., in press*, 1996.

28. N. Tani, T. Ishida, M. Kawano, and K. Kamachi, *Advances in thermal spraying: Proc. 11th Int'l Therm. Spray. Conf.*, p.605, Welding Institute of Canada, Pergamon Press, 1986.

29. S. Tobe, H. Misawa, K. Akita, and Y. Kon, *Proc. 7th Nat'l Therm. Spray Conf.*, Boston, MA, 1994.

30. H. Zhuong and T. Zhang, *2nd Plasma Technik Symp.*, 3:331.

31. R. Knight and R. W. Smith, *Proc. 6th Nat'l Spray Conf.*, pp. 607-612, Anaheim, CA, 1993.

32. W. Reimers, M. Broda, G. Brusch, D. Dantz, K.-D. Liss, A. Pyzalla, T. Schmackers, T. Tschentscher, J. of Non-Destructive Evaluation, 17(3), 1998.

33. Q. Ma and D. R. Clarke, *Acta Metall. Mater.*, 41:1811, 1993.

34. Q. Ma and D. R. Clarke, *Acta Metall. Mater.*, 41:1817, 1993.

35. Thermal Spray Laboratory, State University of New York, Stony Brook, New York.

36. L. B. Freund, *J. Mech, Phys. Solids*, 44:723, 1996.

37. S. Kuroda and T. W. Clyne, *Thin Solid Films*, 200:49, 1991.

38. M. Finot and S. Suresh, *J. Mech. Phys. Solids*, 44:683, 1996.

39. S. Ho and E. J. Lavernia, *Metall. and Mater. Trans. A*, 27A:3241, 1996.

40. F. Kroupa, 5th International Conference on Residual Stresses, Linköping, Sweden, June 1997.

41. F. Kroupa, Z. Knesl, and J. Valach, Acta. Techn. CSAV 38, 29–74, 1993.

42. B. L. Josefson and L.-E. Lindgren, 5th International Conference on Residual Stresses, Linköping, Sweden, June 1997.
43. S. Parthasarathi, B. R. Tittmann, K. Sampath, and E. J. Onesto, *J. Therm. Spray Technol.*, 4:367, 1995.

44. E. F. Rybicki, J. R. Shadley, Y. Xiong, and D. J. Greving, *J. Therm. Spray Technol.*, 4:377, 1995.

45. S. H. Leigh, C. K. Lin, S. Sampath, H. Herman, and C. C. Berndt, *Proc. Int'l Therm. Spray Conf.*, pp. 945-950, Kobe, 1995.

46. C.-C. Chiu and E. D. Case, *Mat. Sci. and Eng.*, A132:39, 1991.

47. C.-C. Chiu, *Mat. Sci. and Eng.*, A150:139, 1992.

48. T. P. Weihs, S. Hong, J. C. Bravman, and W. D. Nix, *Mat. Res. Soc. Symp. Proc.*, 130:87, 1989.

49. M. Finot, O. Kesler, and S. Suresh, *Method and apparatus for the evaluation of a depth profile of thermo-mechanical properties of material and coatings*, U.S. Patent Number 08/675,121, filed July 1996.

50. O. Kesler, M. Finot, S. Suresh, and S. Sampath, Acta Materialia, 45(8), 3123, 1997.

51. S. P. Timoshenko and J. N. Goodier, *Theory of Elasticity*, 3rd. Ed., McGraw-Hill, NY (1970).

52. S. H. Crandall, N. L. Dahl, and T. J. Lardner, *An Introduction to the Mechanics of Solids*, 2nd Ed., McGraw-Hill, NY (1978).

53. A. Pajares, L. Wei, B. Lawn, N. Padture, and C. Berndt, *Mater. Sci. Eng.*, A208:158, 1996.

54. R. V. Hillery, B. H. Pilsner, R. L. McKnight, T. S. Cook, and M. S. Hartle, NASA Contractor Report 180807, 1988.

55. S. Suresh, A. E. Giannakopoulos, and J. Alcala, *Acta Mater.*, 45(4):1307, 1997.

56. R. McPherson, *Proc. 5th Conf. Aluminum Oxide* (Prague, Czechoslovakia: Prague Inst. of Chem. Tech.), 1, 1990.

57. S. Sturlese, R. Dal Maschio, G. Bartuli, N. Zacchetti, and M. Berardo, *High Performance Ceramic Films and Coatings*, ed. P. Vicenzini, Elsevier Science Publish., 353, 1991.

58. P. K. Mallick, *Fiber-Reinforced Composites*, 2nd Ed., Marcel Dekker, NY, 1993.

59. S. F. Wayne, S. Sampath and V. Anand, Tribology Trans., 37(3) 636, 1994.

60. M. Nishida, T. Hanabusa and H. Fujiwara, Surf. Coat. Tech., 61 (1-3), 47, 1993.

61. S. Sampath, H. Herman, N. Shimoda and T. Saito, MRS Bull., 20 (1), 27, 1995.

62. S. Kuroda, Y. Tashiro, and T. Fukushima, Functionally Graded Materials, I. Shiota and M.Y. Miyamoto, Editors, Elsevier Science B. V., 59, 1996.

63. B. H. Rabin, R. L. Williamson, and H. A. Bruck, Functionally Graded Materials, I. Shiota and M.Y. Miyamoto, Editors, Elsevier Science B. V., 387, 1996.

64. A. J. Slifka, A. Kumakawa, J. M. Phelps, and N. Shimoda, Functionally Graded Materials, I. Shiota and M.Y. Miyamoto, Editors, Elsevier Science B. V., 425, 1996.

65. N. Cherradi, D. Delfosse, and P. Moeckli, Functionally Graded Materials, I. Shiota and M.Y. Miyamoto, Editors, Elsevier Science B. V., 379, 1996.

66. D. Delfosse, H.-U. Kunzi, and B. Ilschner, Acta Mater., 40 (9), 2219, 1992.

67. O. Kesler, J. Matejicek, S. Sampath, S. Suresh, T. Gnaeupel-Herold, P. C. Brand, H. J. Prask, Mat. Sci. Eng. A257, 215-224, 1998.

68. I. C. Noyan and J. B. Cohen, Residual Stress - Measurement by Diffraction and Interpretation, Springer-Verlag, New York, 1987.

69. A. J. Allen, M. T. Hutchings, C. G. Windsor and C. Andreani, Advances in Physics, 34 (4), 445, 1985.

70. H. J. Prask and P. C. Brand, Matls. Sci. Forum, 210-213, 155, 1996.

71. G. Simmons and H. Wang, Single Crystal Elastic Constants and Calculated Aggregate Properties: A Handbook, The MIT Press, Cambridge, 1971.

72. H. Behnken and V. Hauk, Z. Metall. 77 (9), 620, 1986.

73. H. P. Klug and L. E. Alexander, X-ray Diffraction Procedures for Polycrystalline and Amorphous Materials; John Wiley & Sons, New York, 1974.

74. J. Matejicek, J. Dubsky and S. Sampath, Proc. United Thermal Spray Conf., Indianapolis, USA, 855, 1997.

75. J. Matejicek, S. Sampath, P. C. Brand and H. J. Prask, Proc. United Thermal Spray Conf., Indianapolis, USA, 861, 1997.

76. S. Kuroda, T. Fukushima and S. Kitahara, Proc. Intl. Thermal Spray Conf., Orlando, USA, 903, 1992.

77. J. Matejicek, S. Sampath and H. Herman, Proc. Intl. Thermal Spray Conf., Nice, France, 1998, *in press.*

78. A. E. Giannakopoulos and S. Suresh, Int. J. Solids Structures, 34(19), 2357-2392, 1997.

79. A. E. Giannakopoulos and S. Suresh, Int. J. Solids Structures, 34(19), 2393-2428, 1997.

80. J. Alcala, A. E. Giannakopoulos and S. Suresh, J. Mater. Res., 13(5), 1998.

81. A. E. Giannakopoulos and P.-L. Larsson, Mechanics of Materials, 25, 1-35, 1997.